First-principles calculations of spin-polarized cation vacancies in wide-gap semiconductors

Dissertation

First-principles calculations of spin-polarized cation vacancies in wide-gap semiconductors

ワイドギャップ半導体中のスピン分極陽イオン空孔に関する
第一原理計算

Graduate School of
Natural Science & Technology
Kanazawa University

Division of Mathematical and Physical Sciences

Student ID Number: 1824012010
Name : Muhammad Yusuf Hakim Widianto
Chief Advisor: Prof. Mineo Saito

First-principles calculations of spin-polarized cation vacancies in wide-gap semiconductors

ワイドギャップ半導体中のスピン分極陽イオン空孔に関する第一原理計算

Muhammad Yusuf Hakim Widianto

Abstract

Vacancy-induced spin-polarized in semiconductors has attracted scientific interests because the applications for spintronics devices. The formation of cation vacancies play important roles of the spontaneous spin-polarization and this is found to raise high-temperature ferromagnetism. We systematically study spin-polarized cation vacancies in wurtzite structure of wide-gap semiconductors, i.e. II-VI (BeO, ZnO, ZnS, CdS) and III-V (BN, AlN, GaN and GaP) by using first-principles calculations based on the density functional theory. We introduce a single vacancy in 128-atoms of wurtzite supercell and find that the spin-polarized C_{3v} symmetry are the most stable. Two (three) majority spin electrons occupy the defect E (E and A_1) levels inducing the magnetic moment 2($3\ _B$) in the case of II-VI (III-V) semiconductors. At the four-anions sites, the spin densities are local-ized and the spin-polarization energies are large in the semiconductors consist of first-row anions (oxygen and nitrogen) due to small atomic radii of oxygen and nitrogen anions. We examine the probability of lowering symmetries distortion from C_{3v} to C_s symmetries and find that the pairing or depairing distortion occurs. This e ect induces split of E level and reduces the spin multiplicity. The energies of symmetry lowering are higher than the spin-polarized state, and thus the most stable structures are spin-polarized C_{3v} symmetry

Key words: Semiconductors, spin-polarized, vacancy, ferromagnetism

Acknowledgements

This Doctoral thesis is a summary of my research during my doctoral program at the Department of Computational Science University Kanazawa University. I intend to convey my deep gratitude for all people who made this research possible, particularly for the guidance and corporation during the past three years.

I would like to give special thanks to my supervisor Prof Mineo Saito for his continuous guidance, motivation, encouragement and support throughout my doctoral research. I am so grateful for having the opportunity to learn and work under supervisor like him with immeasurable knowledge and experience. I will do my best to continue study in computational condensed matter physics elds as a researcher. Hence, I look forward to your continuous support.

I would like to express my gratitude for the examiners of this thesis defence: Prof. Hidemi Nagao, Prof. Taksuki Oda, Prof. Shinichi Miura and Assoc. Prof. Fumiyuki Ishii. They have reviewed and provided feedback throughout all sessions of the defence. Their critical and constructive feedback helps to improve the quality of this thesis.

I would thanks to my collaborative research Hana P. Kadarisman and Amran M. Yatmeidhy. I have received many of their opinions and feedback so this research can be completed in time. Once again, thank you very much for your cooperation and assistance during my research.

My sincere thanks go to all my colleagues and friends who welcome, help and support me since I came here. Very special thanks to Bu Monika, Mas Rifky, Mas Manaf, Pak Teguh, A ah, Dian, Hamid, Nuning, Soca, and Bila for their willingness to be my research discussion as well as joyful friends. Let's continue working hard together.

I also intend to express my gratitude to the Ministry of Education, Culture, Sports, Science and Technology of Japan for providing the MEXT scholarship for the doctoral degree.

Finally, I would like to dedicate this thesis for my beloved wife and families for their support and motivation so that I could conduct and nish this research project.

April 2021

Muhammad Yusuf Hakim Widianto

Research Achievements:

1. M. Y. H. Widianto , H. P. Kadarisman, A. M. Yatmeidhy and M. Saito, Spin-polarized cation monovacancies in wurtzite structure semiconductors: rst-principles study, Japanese Journal of Applied Physics, 59, 071001, June 2020.

Contents

List of Figures

List of Tables

Chapter 1

Introduction

1.1 Spintronics

Integrated circuits (or chips) are building block electronic devices that contain a large amount of semiconductor-based transistors. The quality of the transistor materials plays an important role in enhancing the physical properties. Over the last decades, silicon chips are the most popular to use in transistors based on semiconductors because these materials can work in high-temperature operations and can downsize into several nanometers [1, 2]. However, these materials have been reaching their fundamental limit.

The solution for the above materials is by upgrading the functionality. The materials are added with the degrees of freedom of the electron spin: by the combination of two fundamental properties of electrons (spin and charge), which is now the technology called spin electronics (spintronics). Development of the spintronics materials are expected to increase the function of classic photonic and electronic devices. It can be used for the detection of spin-polarized carriers and transport. Because these materials have multifunctionality, it can be improved overall device performance, for example, by integrating electronic (charge-related) and magnetic (spin-related) operations on single devices. The early generation of spintronics (magnetoelectronics) devices has a bottleneck [3, 4]. In principle, the data is stored in metal-based magnetic devices rst, and then it is processed in

semiconductor-based electronic devices that can be increased the cost of time and energy. Integrating both functionalities in one system is expected to increase the speed and energy efficient. The alternative is used materials with combine ferromagnetic and semiconducting in one system.

1.2 Dilute Magnetic Semiconductors

Ferromagnetism and semiconducting are observed to coexist in some materials. Since the discovery of ferromagnetism in semiconductors, much effort has been concerned to use dilute magnetic semiconductors (DMS) materials [5, 6, 7]. These materials combine the functionality of semiconductors and ferromagnets and thus can be applied for spintronics devices. Figure 1.1 shows the schematic representation of conventional semiconductor and DMS materials. It has been suggested that DMS materials improve the novel properties for nonvolatile memories, decreased power consumption, increased the processing speed of the devices, and possibly smaller structures [8]. A key of issue is the development of DMS materials which is using the spin-polarized carriers. Hence, one primary goal in the research of DMS materials is to develop magnetic semiconductor above room temperature. The understanding of physical properties of these materials is necessary.

DMS materials have two main classes: (1) DMS based impurity and (2) DMS based vacancy [5, 9, 10]. In the case of impurity-DMS, the semiconductor materials are doped with magnetic atoms that include d or f atomic orbitals. In general, the impurity atoms are located on substitutional and interstitial sites of the semiconductor host. DMS based on the impurity is one of the promising candidates for implementation in spintronics devices. However, these materials are found that have below room temperature magnetism [11, 12, 13].

Recently, the most attention of vacancy-induced magnetism of DMS materials has been focused on wide-gaps semiconductors. The discovery vacancy-induced ferromagnetism in thin film of HfO_2 have much atten-

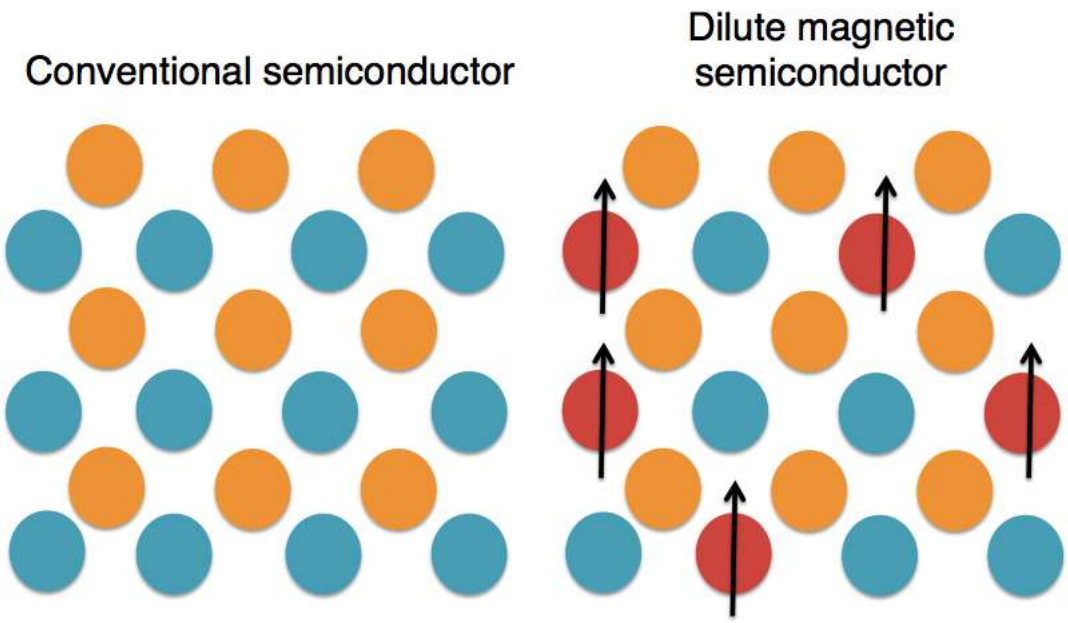

Figure 1.1: Schematic representation of conventional semiconductor and dilute magnetic semiconductor. The arrows represent the domain with orientated spin-polarization.

tion because these materials is one of the wide-gap semiconductors and is observed that have high-temperature of magnetism (400 K) [14, 15, 16]. The magnetism behavior possibly due to the presence of the small concentration of intrinsic point defects in thin lm of HfO_2 [17, 18, 19]. This phenomenon leads to the new generation of magnetism without the localized d or f atomic orbitals. It classi es as d^0 ferromagnetism, which is commonly found in semiconductors.

The d^0 ferromagnetism is also found in various undoped of wide-gaps semiconductors, i.e, nitrides (AlN [20], BN [21], and GaN [22]) and oxides (TiO_2 [18], SnO_2 [23], ZnO [24, 25], CuO [26] and MgO [27]). Madhu et al. [22] was observed the room-temperature ferromagnetism (390 K) in the bulk of GaN. The magnetism is caused by intrinsic defects such as Ga vacancy in GaN lms. By spin-polarized positron annihilation spectroscopy (SP-PAS), Maekawa et al. [28] was observed that the ferromagnetism occurs at 300 K in GaN lm due to Ga vacancies. When the temperature reaches 30 K, the ferromagnetism vanish in GaN case. In the case of GaP, the experimental study by using Electron Paramagnetic Resonance (EPR) at 20 K was found that Ga vacancy reveals spin $\frac{3}{2}$ [29]. This magnetism behavior indicates that the spontaneous spin electrons appear at room tem-

peratures in the case of III-V semiconductors. Therefore, study the mechanism of spontaneous spin polarization in the III-V semiconductors are necessary.

The experimental study by using SP-PAS was observed that vacancy-induced ferromagnetism is also found in the oxides case such as ZnO [30]. Zn vacancies are suggested to introduce the magnetism in bulk ZnO. The magnetization increases in the high temperature and decreases when reach 100 K. It indicates that the Curie temperature is higher than room temperature in the case of Zn vacancy in ZnO [31]. Several investigations of magnetism in oxides propose that the unpaired atoms near vacancies induce the spin polarization [32]. As result, ZnO posses the high-spin state with $S = 1$, which is related to the neutral Zn vacancy [33]. Those conditions have been predicted by using electron paramagnetic resonance [34]. Other II-VI semiconductors (ZnS [35] and CdS [36]) was also observed and predicted that the cation vacancies cause magnetism in low-temperature. Therefore, study the mechanism of spin-polarized in II-VI semiconductors can be improved our understanding.

1.3 Density Functional Theory in DMS Material

Theoretical calculations based on density functional theory (DFT) have been increased to study the mechanism of atomic structures. The study of spin-polarized within the framework of DFT are powerfully used to analyze vacancy-induced magnetism in semiconductors. Spin-polarized DFT can be described the magnetism of itinerant electrons in solid state materials.

By DFT calculations, El mov et al. [37] study CaO bulk and nd that the magnetism due to strong interaction in the atoms near vacancies of Ca. First-principles calculation of electronic structure on TiO_2 [38] and HfO_2 [17] are showed that isolated cation vacancies induce the formation of the high-spin state as the ground state. It also predicts in other materials such as V_2O_5 [10], BeO [39], ZnS [40], ZnSe [41], ZnTe [41], GaN [33, 42, 43],

GaP [33], AlN [33], and BN [22]. On those systems, cation vacancies are theoretically predicted to cause spontaneous polarization. The atomic spin polarization are strongest and localized for rst row anions like N or O [33, 44]. The atoms near vacancies is predicted to form sp^n hybridization electronic state and the magnetism is induced d^0 system without localized d or f atomic orbitals. Therefore, it is important to study the mechanism of vacancy-induced spin-polarization in wide-gap semiconductors based on rst-principles calculations.

1.4 Purpose of Study

It has been recognized that the cation vacancy in II-VI and III-V semiconductors cause spontaneous spin-polarization. Theoretical calculation based on DFT is reliable eect to study these mechanism. In this work, we focus on semiconductors-based cation vacancy systems aiming the detailed description of their structural and magnetic properties. We systematically study the spin-polarized cation vacancies in wide-gap of wurtzite structure semiconductors, i.e, II-VI (BeO, ZnO, ZnS, CdS) and III-V (BN, AlN, GaN, and GaP). The rst goal is to understand the mechanism of spin-polarized cation vacancies in II-VI and III-V semiconductors where investigation of the stable structure and ground states are necessary. The ground states are aected by the stability of geometries and the origin of the large spin density is due to the physical properties of atoms near-vacancies sites. The stable spin state is also necessary to study. We study the chemical trend of anions because the high transition temperature is found for oxides and nitrides. We nd that the most stable structures in a single vacancy of wurtzite structures are spin-polarized and C_{3v} symmetry. In the case of II-VI semiconductors, the defect E level is occupied and unoccupied by the majority and minority spin electrons cause the magnetic moment is 2 $_B$. The magnetic moment is 3 $_B$ in the case of III-V semiconductors due to the fact that the defect E and A_1 level are occupied (unoccupied) by majority (minority) spin electrons.

We next examine the possibility of the symmetry lowering in a single vacancy of wurtzite structures which reduces the spin multiplicity. The geometries structure in the wurtzite supercell with a single cation vacancy are reduced from the high symmetry C_{3v} to the lower symmetry C_s. The energy gain induce by the symmetry lowering is small, therefore the most stable structure is spin polarized C_{3v}.

1.5 Outline of Dissertation

This dissertation consists of five chapters. This PhD thesis partly follows an article-based style in which it includes complete manuscripts which have been published by the author (as presented in the Research Achievements). The background of this research is introduced in Chapter 1. In Chapter 2, we explain the basic concepts of first-principles calculations based on density functional theory. Chapter 3 presents the subject of our result and discussion of the study cation vacancies in wurtzite supercell. In chapter 4, we discuss the effect of symmetry lowering which reduces the spin multiplicity. Finally, in Chapter 5, we give our concluding remarks.

We introduce the character table of the symmetry in Appendix A. We explain and simplify the model of the wavefunctions of four-anions dangling bonds in Appendix B.

Chapter 2

Theoretical Background

In this chapter, we explain a brief overview of the concept density functional theory (DFT). First, we give a brief explanation of the basic concept of DFT in Section 2.1. We describe spin-polarized calculations within the framework of DFT in Section 2.3. In Section 2.4, we use group theory representation to analyze the localized state of band structures at k point of rst Brillouin zone (FBZ). Next we explain the application of DFT in Section 2.5.

2.1 Density Functional Theory (DFT)

One of the most popular calculation methods in solid-state physics and quantum chemistry are density functional theory (DFT). This calculation method describes the interaction electron system in the form of electron density. DFT calculation requires less computational cost and good accuracy compared with the Hartree-Fock. The idea of DFT is based on the two theorem from Hohenberg-Kohn[45].

2.1.1 Hohenberg-Kohn Theorems

The idea of Hohenberg-Kohn (HK) can be assumed as two functional theorem. The rst theorem as follow:

Theorem 1. The ground state of electron density $\rho_0(\mathbf{r})$ for any system of

interacting particles in some external potential $V_{ext}(r)$ determines this potential unique functional.

Proof. The first theorem can be proved by reductio ad absurdum. Let assume that two system of electrons have different external potential $V_1(r)$ and $V_2(r)$ in which lead to the same ground-state electron density $n_0(r)$. The two external potentials ($V_1(r)$ and $V_2(r)$) have two different Hamiltonian ($\hat{H}_1$ and $\hat{H}_2$) and also have two different ground state wavefunctions ($_1$ and $_2$). Hypotetically, the two wavefunctions ($_1$ and $_2$) have the same ground-state electron density $n_0(r)$ but different ground state of energy. Since $_2$ belong to $\hat{H}_2$ and it does not related with $\hat{H}_1$, it follow that:

$$E_1 = h\ _1|\hat{H}_1|\ _1i < h\ _2|\hat{H}_1|\ _2i : \tag{2.1}$$

The last term in 2.1 can be written as

$$h\ _2|\hat{H}_1|\ _2i = h\ _2|\hat{H}_2|\ _2i + h\ _2|\hat{H}_1 \quad \hat{H}_2|\ _2i = E_2 + \int d^3r\,[V_1(r) \quad V_2(r)]\,n_0(r) \tag{2.2}$$

then we can obtain

$$E_1 < E_2 + d^3r\,[V_1(r) \quad V_2(r)]\,n_0(r); \tag{2.3}$$

We can find for E_2 by using the similar expresion Eq.2.3, as follow:

$$E_2 < E_1 + d^3r\,[V_1(r) \quad V_2(r)]\,n_0(r); \tag{2.4}$$

If we add the Eq.2.3 and 2.4, this summation obtain inconsistency $E_1 + E_2 < E_1 + E_2$. This inequality shows that it is impossible to have two different external potential inducing the same non-degenerate ground-state charge density and thus the theorem is proved by reductio ad absurdum.

The second theorem of Hohenberg-Kohn is explained as:

Theorem 2. For any particular $V_{ext}(r)$, a universal functional occur for the total energy functional $E[n]$ that its global minimum value provides the

exact ground state energy of the system, and the density $n(r)$ that minimizes the functional is the exact ground state density $n_0(r)$.

Proof. All properties can be indenti ed as a functional $n(r)$; include the total energy functional, therefore the Hohenberg-Kohn energy functional can be written as[45]

$$E_{HK}[n] = T[n] + E_{II} + E_{int}[n] + \int V_{ext}(r)n(r)d^3r; \qquad (2.5)$$

where $T[n]$ is kinetic energy, E_{II} is interaction energy of nuclei, and $E_{int}[n]$ is potential energy of the interacting system. Since $T[n]$ and $E_{int}[n]$ are the same for all systems, we obtain to be the universal functional $F[n]$, it can be written as

$$E_{HK}[n] = F[n] + E_{II} + \int V_{ext}(r)n(r)d^3r; \qquad (2.6)$$

The system is considered with the ground state density $n_1(r)$ coressponding to external potential $V_1(r)$, which is given by

$$E_1 = E_{HK}[n_1] = h\ _1|\hat{H}_1|\ _1i : \qquad (2.7)$$

For the di erent density $n_2(r)$ corresponding to a di erent wavefucntion $_2$, we get

$$E_2 = h\ _2|\hat{H}_1|\ _2i : \qquad (2.8)$$

It follows that the energy E_2 is larger than E_1, since

$$h\ _1|\hat{H}_1|\ _1i < h\ _2|\hat{H}_1|\ _2i : \qquad (2.9)$$

We can minimize the energy E_2 with correspond to electron density $n(r)$ and express the total energy as a function of electron density until gain the ground state energy. The ground-state of the system is the minimal value of $E_{HK}[n]$. However, the problem still remains that $E_{HK}[n]$ is unknown.

2.1.2 Kohn-Sham Equation

The Kohn-Sham (KS) equation belong to the fundamental concept of DFT. The KS uses the HK theorem which is already explained in the previous section. The total energy of the system depends on the electron density of the system in the case of KS equation. The statement is expressed as

$$E = E[n(r)] : \tag{2.10}$$

The basic idea is from the mapping of interaction of the electrons system in to an auxiliary system of a non-interacting electrons with the same ground-state of electron density $n(r)$. The ground-state of electron density is represented as the sum of all electron orbitals for the system of non-interacting electrons, it can be expressed as follow

$$n(r) = \sum_{i}^{M} |\psi_i(r)|^2; \tag{2.11}$$

where i runs from 1 to $M/2$ if we consider double occupacy of all states. The electron varies by changing the trial wavefunction of the system. The whole system is ground state if the electron density belong to the minimum energy. We can find the ground state density and energy by solving KS equation. This calculation has depended on the accuracy of the exchange and correlation interaction.

By introducing the effective potential (the external potential, Coulomb interaction between electrons, and the exchange-correlation interactions), the interaction-electron case replaces with the non-interaction electron case in the KS approach. Hence, the KS equation for the ground state can be expressed as[46]

$$E_{KS}[n] = T_s[n] + E_H[n] + E_{XC}[n] + \int V_{ext}(r)n(r)d^3r; \tag{2.12}$$

where $T_s[n]$ is the kinetic energy of non-interaction electrons and is ex-

pressed as

$$T_s[n] = \sum_i \int \frac{\hbar^2}{2m} \nabla^2 \psi_i(r)\, \psi_i(r)\, dr : \qquad (2.13)$$

The second term is Hartree energy E_H which consist of the electrostatic interaction:

$$E_H[n] = \frac{e^2}{2} \int \frac{n(r)n(r')}{|r - r'|} dr\, dr' : \qquad (2.14)$$

As the explanation above, we can group the exchange and correlation interactions into the exchange-correlation energy E_{xc}. We can find the ground state electron density and the ground state of total energy by using E_{xc}.

Kohn-Sham equation based on the many-body Schrödinger equation can be obtained by applying variational theorem of the energy functional E_{KS} with respect to the wavefunctions. The equation can be written as

$$\left[-\frac{\hbar^2}{2m} \nabla^2 + V_{eff}(r) \right] \psi_i(r) = \varepsilon_i\, \psi_i(r): \qquad (2.15)$$

The Kohn-Sham equation is defined by a local effective potential V_{eff} in which the non-interacting particles move. The effective potential then can be write as[46]

$$V_{eff}(r) = V_{ext}(r) + V_{XC}(r) + V_H(r); \qquad (2.16)$$

with

$$V_H(r) = \frac{e^2}{2} \int \frac{n(r')}{|r - r'|} dr' : \qquad (2.17)$$

The kinetik energy is given by

$$T[n(r)] = \sum_i \varepsilon_i - \int V_{eff}\, n(r)\, dr : \qquad (2.18)$$

The total energy of the KS equation is given by

$$E_{KS}[n] = \sum_i \varepsilon_i + E_{XC}[n] + \frac{1}{2} \int \int \frac{n(r)n(r')}{|r - r'|} dr\, dr' - \int V_{eff}(r)\, n(r)\, d^3r \qquad (2.19)$$

Since the Hartree term and V_{xc} depend on $n(r)$, which is depend on ψ_i,

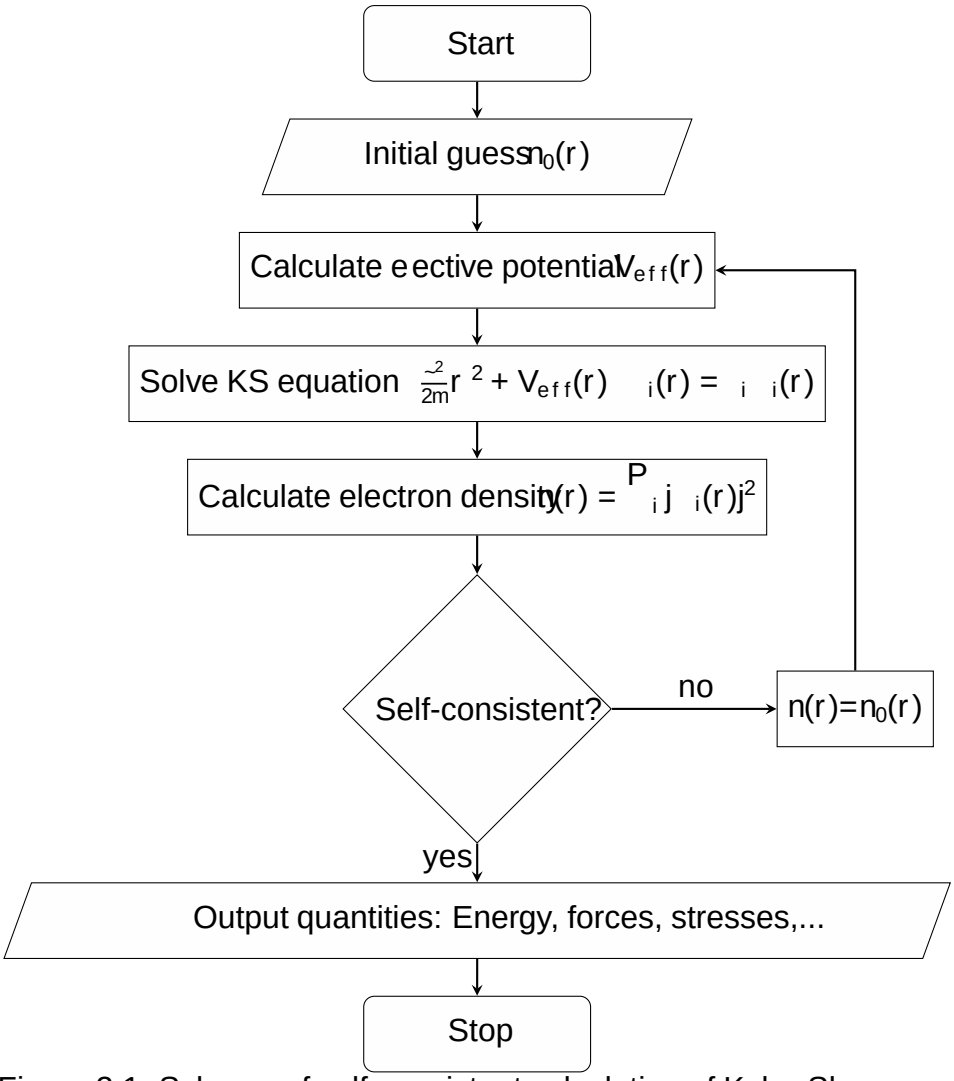

Figure 2.1: Scheme of self-consistent calculation of Kohn-Sham equations.

the KS equation should be solved in an interative self-consistent way. The iterative procedure is drawn as ow chart in Fig. 2.1.

2.2 Exchange and Correlation Functional

The KS equation cannot be solved since the exact functional $E_{xc}[n]$ is still unknown. Hence, he accuracy of exchange-correlation energy $E_{xc}[n]$ (or potential $V_{XC}(r)$ functional) is needed to describe the solid-state system. The most use for $V_{XC}(r)$ are Local Density Approximation (LDA) [47, 48] and Generalized Gradient Approximation (GGA) [49]; The LDA functional is based on the approximation on homogeneous electron gas (HEG) and the GGA functional expand the functional by adding the gradient term. We can write the exchange correlation of LDA functional V_{XC}^{LDA} as:

$$V_{XC}^{LDA} = \varepsilon_{XC}(n(r)) + n(r)\frac{\partial \varepsilon_{XC}(n(r))}{\partial n(r)}: \qquad (2.20)$$

We can express the GGA functionals for exchange-correlation potential as:

$$V_{XC}^{LDA} = \varepsilon_{XC}(n(r)) + n(r)\frac{\partial \varepsilon_{XC}(n(r))}{\partial n(r)} \quad r \quad n(r)\frac{\partial \varepsilon_{XC}(n(r))}{\partial \nabla n(r)}\Bigg)^{!} : \qquad (2.21)$$

The Kohn-Sham equation then can be solved self-consistently as shown in the gure 2.1. Our calculation is focused by using GGA.

2.3 Spin-Polarized Calculations

We here adopted the spin-polarization calculations from several materials [50, 51, 52]. Barth and Hedin[50] were calculated the spin-polarized case by extension the DFT. As the description above, the DFT calculates the non-spin polarized (non-magnetic) systems. In principle, the magnetic system can be applied to rst-principles calculations based on density functional theory: the spin polarization induce to magnetization density $m(r)$, since the magnetization is functional $m[n(r)]$ of ground state charge density $n(r)$. We explain the upaired electrons by understanding the electronic

state. On the case of non-spin polarized, the spatial orbitals $\psi(r)$ are restricted to be the same for opposite spins. On the other hand, Up and down spins in each electron pair have different spatial orbitals (spin-up $\psi^{\uparrow}(r)$ and spin-down $\psi^{\downarrow}(r)$) and energies, as shown in Fig. 2.2.

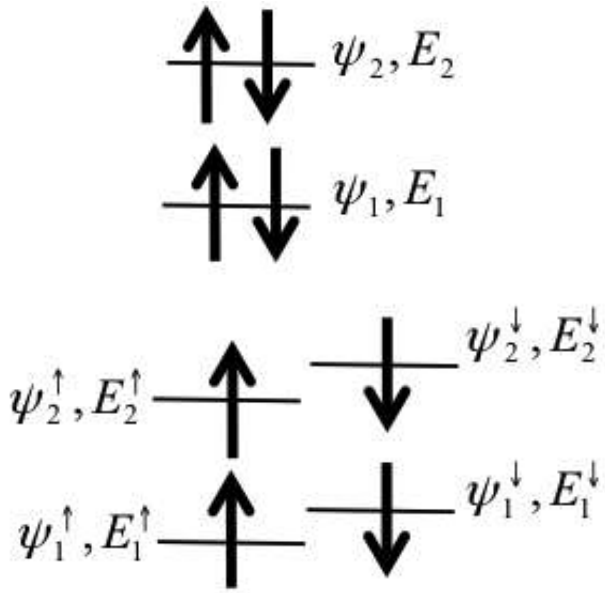

Figure 2.2: Schematic representation of non-spin polarized (upper-part) and spin-polarized (lower-part).

We calculate the spin density as:

$$n(r) = n_{\downarrow}(r) \quad n_{\uparrow}(r) = \sum_{i=1}^{N_{\uparrow}} \psi_i^{\uparrow}(r)^2 \quad \sum_{i=1}^{N_{\downarrow}} \psi_i^{\downarrow}(r)^2 : \qquad (2.22)$$

The total density is calculated as:

$$n(r) = n_{\downarrow}(r) + n_{\uparrow}(r) = \sum_{i=1}^{N_{\uparrow}} \psi_i^{\uparrow}(r)^2 + \sum_{i=1}^{N_{\downarrow}} \psi_i^{\downarrow}(r)^2 : \qquad (2.23)$$

Because the magnetization density is functional $m[n(r)]$ of ground state charge density $n(r)$, we calculate the moment magnetic as:

$$m(r) = \mu_B \, n_{\uparrow}(r) \quad n_{\downarrow}(r) : \qquad (2.24)$$

2.4 Group Theory Representation in Band Structure

The group theory is used to understand the irreducible representation of occupied state on the several band structure at some point of first Brillouin zone. In our calculations, we use the finite size of supercell and find that the band dispersion of defect level arises artificially. When the structure becomes lower symmetry, the band splits and analyze the occupied state of the splits band are necessary. We here explain the theoretical background of group theory.

The symmetry operation $\hat{R}_i$ is expressed as:

$$\hat{R}_i = \{\hat{\ }_i | \tilde{\tau}_i\} \tag{2.25}$$

where $\hat{\ }_i$ is rotation and $\tilde{\tau}_i$ is fractional translation. The Bloch wavefunction, $\ ^k_i(\tilde{r})$, is defined as[53][54]

$$\ ^k_i(\tilde{r}) = \frac{1}{\sqrt{NV}} e^{i\tilde{k}\cdot\tilde{r}} \sum_n c_j(\tilde{G}_n) e^{i\tilde{G}_n\cdot\tilde{r}}; \tag{2.26}$$

where $\tilde{G}_n$ is a reciprocal lattice vector and $\tilde{k}$ is a wave vector in the first Brillouin zone. $c_j(\tilde{G}_n)$ is a coefficient and the band index j is in the ascending order of energy. The total number and volume of each unit cell represents N and V, respectively. The irreducible representations of wavefunctions are determined by evaluating the following expression:

$$Q = \frac{1}{l} \sum_i (\hat{R}_i) \langle\ | \hat{R}_i | \ \rangle; \tag{2.27}$$

where l is the order of the group and $(\hat{R}_i)$ is the character of the irreducible representation of and i runs over the symmetry operations of the k group. The wavefunctions belong to (do not belong) the irreducible representation when $Q = 1$ ($Q = 0$). By using 2.26 and 2.27, the equation is written as:

$$Q = \sum_i \acute{\ }(\hat{R}_i) \sum_n c_j(\tilde{G}_n) c_j(\hat{\ }_i \tilde{G}_n - \acute{\tilde{G}}_n) \quad e^{(-i(\hat{\ }_i \tilde{G}_n - \acute{\tilde{G}}_n)\cdot\tilde{\tau}_i)}; \tag{2.28}$$

where $\vec{k}$ satis es $\hat{R}_i\vec{k} = \vec{k} - \vec{G}_i$ for a given reciprocal lattice vector $\vec{G}_i$ ($\vec{G}_i = 0$ when the $\vec{k}$ point is inside the rst Brillouin zone). The irreducible ray representations character is given by:

$$\chi(\hat{R}_i) = e^{(i\vec{k}\cdot\vec{\tau}_i)}\,\chi(\hat{R}_i): \tag{2.29}$$

The irreducible representations in the most cases belong to those of the conventional irreducible representation of the point groups. In here, we use the Mulliken symbol to express these representations. However, insome exceptional cases, the irreducible ray representations do not belong to unconventional irreducible representations as mentioned in the paper[55, 56, 57, 58]. We implement this method in the rst-principles calculation PHAOSE code[59], and the irreducible representation in the band structure then can be identi ed directly from the result of DFT calculations.

2.5 Calculation Methods

We explain the basis of the DFT in the previous section. DFT can be applied to calculate the lattice constant, band structure, density of state and so on. We here present the application of the DFT in the crystal and supercell systems.

2.5.1 Lattice Constant Optimization

The lattice constant optimization is required in the DFT calculations. We optimize the lattice constant and atomic position of the wurtzite structure. Wurtzite have four atoms per hexagonal unit cell. The unit vectors are $\vec{a} = (\frac{1}{2}; \frac{\sqrt{3}}{2}; 0)a$, $\vec{b} = (\frac{1}{2}; -\frac{\sqrt{3}}{2}; 0)a$, and $\vec{c} = (0; 0; c)$, where a and c are the wurtzite lattice constant. The position of the two cation atoms are $(\frac{1}{3}; \frac{2}{3}; 0)$ and $(\frac{2}{3}; \frac{1}{3}; \frac{1}{2})$ and the position for two anion atoms are $(\frac{1}{3}; \frac{2}{3}; u)$ and $(\frac{2}{3}; \frac{1}{3}; \frac{1}{2} + u)$, where u is internal parameter. The ideal wurtzite have the value of u is $\frac{3}{8}$ and $\frac{c}{a} = \sqrt{\frac{1}{u}}$.

The equilibrium geometry of the wurtzite is obtained by first using ideal wurtzite geometry parameter and vary the lattice constant a to get the equilibrium of a. We next keep the last lattice constant a and internal parameter u is ideal and vary the c/a ratio to get the new optimized c/a value. We once again vary the lattice constant a with the new c/a to determine new equilibrium of the lattice constant a. We last vary the internal parameter u by keep the value of a and c/a ratio. Tabel 2.1 and Fig.2.3 shows the optimized lattice constants for pristine wurtzite structures of BN, AlN, GaN, GaP, BeO, ZnO, ZnS and CdS, in which wurtzite structure is C_{6v} symmetry.

Table 2.1: Optimized geometries and lattice constants of pristine wurtzite. The units of the bond angles ($_x$) and bond lengths (r_x) are degree and amstrong (Å), respectively. The E_g is direct gap semiconductors where both the minimum conduction and maximum valence bands are located at the point within the units is eV.

Systems	a (Å)	c (Å)	c/a	u	$_1$	$_2$	r_1	r_2	r_3	E_g
BN	2.559	4.239	1.657	0.378	109.8	109.1	1.570	1.588	2.559	5.33
AlN	3.145	5.029	1.599	0.382	108.1	110.8	1.910	1.912	3.145	3.89
GaN	3.144	5.119	1.629	0.377	109.6	109.8	1.921	1.931	3.144	2.67
GaP	3.842	6.335	1.649	0.381	109.7	109.2	2.357	2.369	3.842	1.56
BeO	2.718	4.389	1.615	0.380	108.8	110.1	1.658	1.660	2.718	7.32
ZnO	3.305	5.285	1.599	0.383	108.2	110.7	2.009	2.016	3.305	0.65
ZnS	3.909	6.349	1.624	0.379	109.2	109.8	2.398	2.390	3.910	1.93
CdS	4.332	6.745	1.557	0.384	107.2	111.7	2.618	2.600	4.332	0.98

We carry out first-principles calculations based on the density functional theory for the above methods. We use the first-principles calculation of PHASE/0 code[59], where ultrasoft pseudopotentials and plane waves are used. The generalized gradient approximation [49] is used as exchange-correlation functionals. We use the 15 15 15 of k-points mesh and the optimized geometries is under the condition that the atomic forces are less than 0.005 eVÅ^{1}. The cutoff energies of the wavefunctions is 25 Rydberg and charge density is 225 Rydberg.

2.5.2 A Single Vacancy in Wurtzite Supercell

Fig.2.4 and Table2.2 show the geometry optimized of single cation vacancy in the 128-atoms of wurtzite supercell of BN, AlN, GaN, GaP, BeO, ZnO,

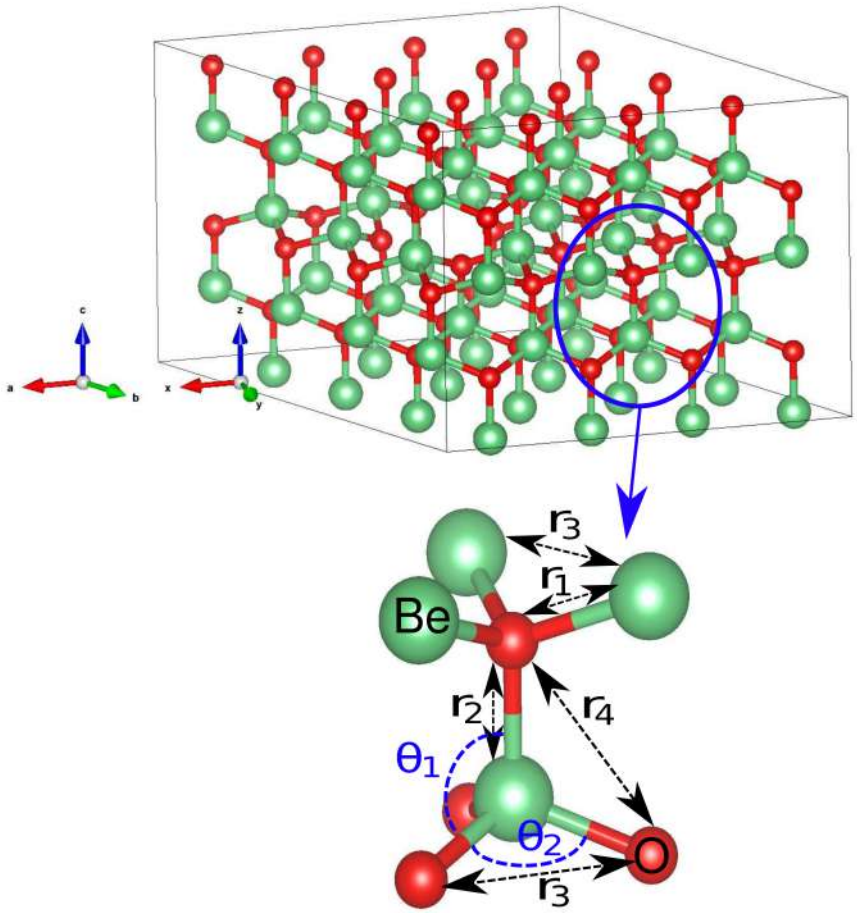

Figure 2.3: Atomic structure of pristine wurtzite supercell C_{6v} symmetry (upper part). In unitcell case, the atomic distances (r_1, r_2 and r_3) and bond angles ($_1$ and $_2$) are de ned (down part) and these values are tabulated in Table 2.1.

Table 2.2: Optimized geometries of single cation vacancy. The parameters: atomic distances (r_a and r_b) and bond angles ($\bar{\ }$) are de ned in Figure 2.4. The average value of the three bond angles of the rst anion represents $\bar{\ }$ in Fig. 2.4.

Systems		$\bar{\ }$	r_a (Å)	r_b (Å)
V_{Be} in BeO	115.2	116.6	3.022	2.971
V_{Zn} in ZnO	116.0	116.7	3.647	3.588
V_{Zn} in ZnS	109.5	110.5	3.944	3.890
V_{Cd} in CdS	112.4	113.1	4.560	4.293
V_B in BN	114.1	114.1	2.798	2.822
V_{Al} in AlN	116.1	117.4	3.509	3.444
V_{Ga} in GaN	115.0	115.0	3.434	3.431
V_{Ga} in GaP	107.6	107.4	3.595	3.653

ZnS and CdS. We use the cut energies (cuto energies of the wavefunctions and charge density) which is the same as optimized geometries of unitcell. For calculation in the supercell, we decrease k-points and

use the 3 3 3 of k-points mesh. We check the geometry stability by increasing the k-points until 7 7 7 of mesh and nd that the optimized of bond angles and bond lengths are well convergence. The study of geometry stability in cation vacancies are discussed in the next section. We use the atomic forces as the same as optimized geometries of unitcell.

We analyze the wavefunctions at the point at the rst Brillouin zone of the supercell and clarify the irreducible representations of the defect levels. We use a projection operator method to identify the irreducible representations of the defect levels, which was described in previous papers[55, 56, 57, 58].

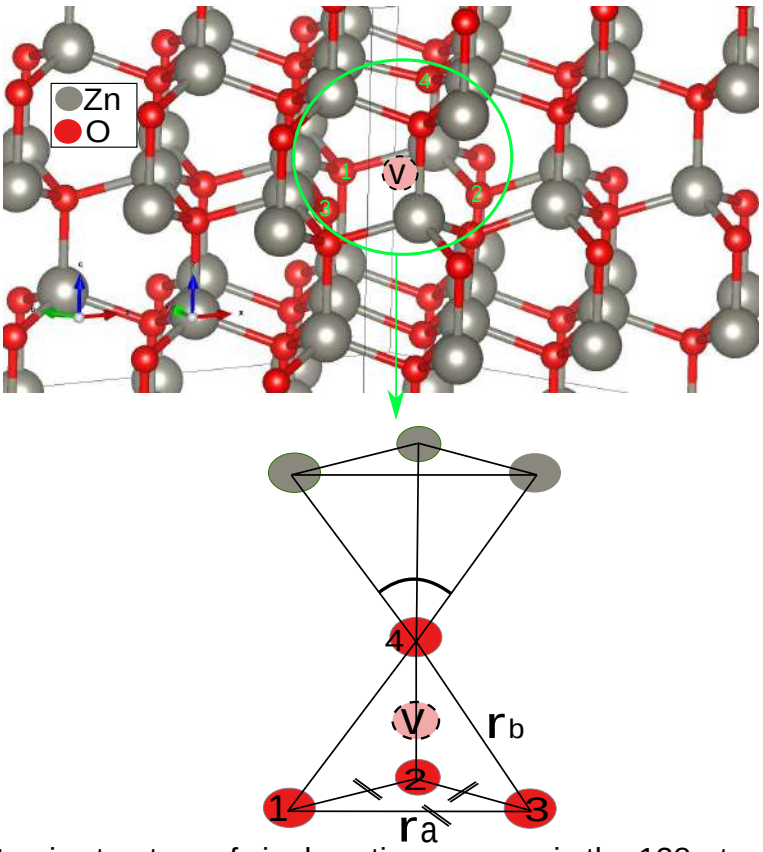

Figure 2.4: Atomic structure of single cation vacancy in the 128-atoms of wurtzite supercell (upper part). The atomic distances of anion-anion r_a and r_b, and bond angles α, are de ned (dow part) and these values are tabulated in Table 2.2.

Chapter 3

Spin-Polarized Cation Vacancy in Semiconductors

In this chapter, we study the electronic properties of single cation vacancy of wurtzite supercell. We examine the stability of geometries structures in the supercell due to increasing of k-point. We also discuss the atomic structure of single cation vacancy of wurtzite 128-atoms supercell by considering the bond lengths and bond angles of the atoms near vacancies. We clarify the most stable of the geometry structures at the ground state. We use the group theory to analyze the band structure at the k-point in First Brillouin zone.

3.1 Convergence of supercell

We observe the convergence of supercell by calculating the spin polarization energy in 128, 256 and 512 atoms of supercell (Table 3.1). We find that the system is well converge. The atomic distance between anions (r_a and r_b) near vacancies have found slightly different when the system become large (512 atoms). The spin polarization energy E_{sp} is found well convergence.

Table 3.1: Convergence of supercell in GaN and ZnO. The parameters: atomic distances (r_a and r_b) and spin polarization energy (E_p)

System	Supercell	r_a	r_b	E_p (eV)
V_{Ga} in GaN	128	3.434	3.431	0.481
	256	3.443	3.440	0.481
	512	3.451	3.444	0.470
V_{Zn} in ZnO	128	3.647	3.588	0.043
	256	3.647	3.592	0.036
	512	3.648	3.617	0.035

3.2 Geometries Stability

We study the geometry stability of a single cation vacancy due to increasing the k-point mesh in which the supercell size is constant (128-atoms), as shown in Table 3.2. We here use several k-point mesh and study the geometry stability of a single cation vacancies GaN. After the convergence atomic force is less than $5 \cdot 10^{-3}$ eVÅ^{-1}, we find that the value of the stability of geometries are close each other: the optimized of bond angles (θ) and atomic distance (r_a and r_b) are well convergence, as Table 3.2 shows. Since the bond angles and bond lengths have adjacent values, we here use 3 3 3 k-point mesh due to reducing the computational cost. We conclude that geometry is found to be stable when k-point gradually increased and the vary of these values are very small.

Table 3.2: Geometry stability of GaN and ZnO in the several k-point. The parameters: atomic distances (r_a and r_b) and bond angles (θ) are defined in Figure 2.4

System	Kpoint mesh			θ	r_a	r_b
V_{Ga} in GaN	3	3	3	114.97	3.434	3.431
	4	4	4	114.95	3.436	3.437
	5	5	5	114.96	3.441	3.439
	7	7	7	114.96	3.442	3.434
V_{Zn} in ZnO	3	3	3	116.10	3.647	3.588
	7	7	7	116.48	3.648	3.617

3.3 Cation Vacancies in II-VI Semiconductors

The first discussion is the cation vacancies in II-VI semiconductors, where in this calculations we use oxides (BeO and ZNO) and sulfides (ZnS and CdS) semiconductors, respectively. In the case of oxide semiconductors (ZnO and BeO), we find that the most stable structures are C_{3v} symmetry and are spin polarized. The density of states (DOS) in Fig. 3.1 shows the defect A_1 level of the minority spin is located just below the Fermi level on the case of BeO. Unoccupied state of the defect E level of the minority spin is located above the Fermi level; we identify the irreducible representations of the above mentioned level by analyzing the wavefunctions at the point in the supercell. We find that the calculated of magnetic moment is $_B$ 2 since the defect E level occupy by only majority spin electrons. We note that the defect level in DOS is somewhat broad, which due to by the fact that the finite size of the supercell, then the band dispertion of the defect level appears artificially. The dispertion becomes small when using a large supercell.

We find that the magnetic moment is 1.71 $_B$ in the case of single cation vacancy of ZnO 128-atoms supercell. The non-integer value is originated due to the finite dispersions of the defect A_1 and E levels as the DOS in Fig 3.1 shows. By using substantially large supercell (512-atoms), the magnetic moment is close to the integer (2 $_B$) because the defect level becomes narrower. We study the wurtzite 256- and 512-atoms supercell and find that the magnetic moments are 1.84 $_B$ and 1.99 $_B$ for 256- and 512-atoms, respectively, which is close to the integer value. The defect E level in ZnO is found to be narrower as in the DOS Fig.3.2. In the other theoretical calculations, the non-integer values of the magnetic moments were also achieved.[60].

We find that the atomic distance of oxygen-oxygen in ZnO case r_a and r_b (Fig. 2.4) is 10.3% and 10.1% larger than the ideal value (the value in the pristine crystal as seen in Table 2.1), respectively, and this is due to the outward relaxations of the four oxygen atoms. r_a is 11.2% and r_b is 10.1%

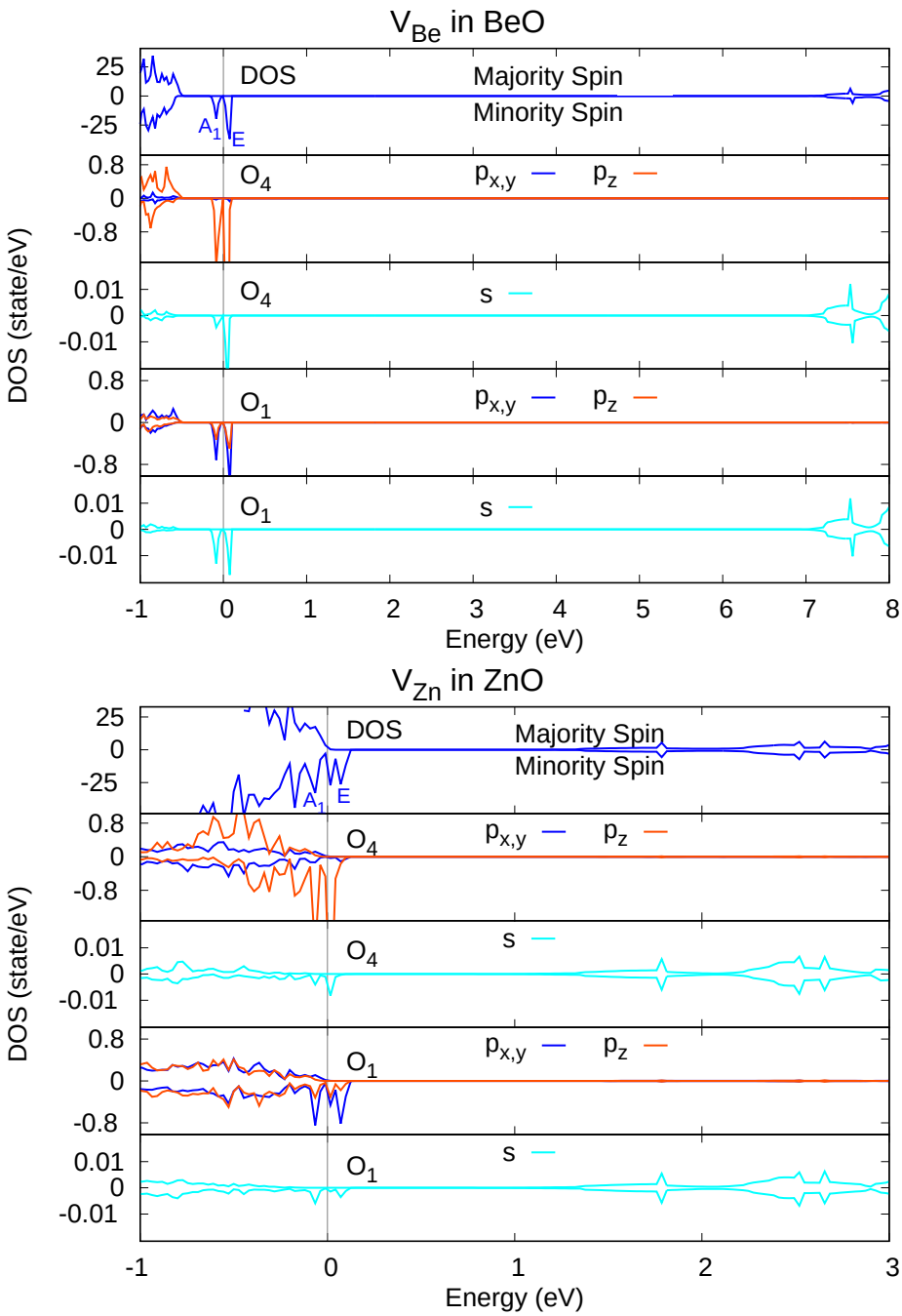

Figure 3.1: DOS and PDOS for the 1st and 4th atoms near cation vacancy in the case of BeO (upper part) and ZnO (lower part) which are de ned in Figure 2.4. The Fermi level represents vertical grey line.

larger than the ideal distance of BeO (Table 2.2). At the near four oxygen atoms, the bond angles become larger than sp^3 hybridization angle (109.5) as Table 2.2 shows; The bond angle(s) are 115.2 (116.6) for BeO and 116.0 (116.7) for ZnO, where the and ¯ are the bond angle of the fourth anion and the average value of the three bond angles of the rst anion, respectively (The locations of atoms for the rst and fourth anions

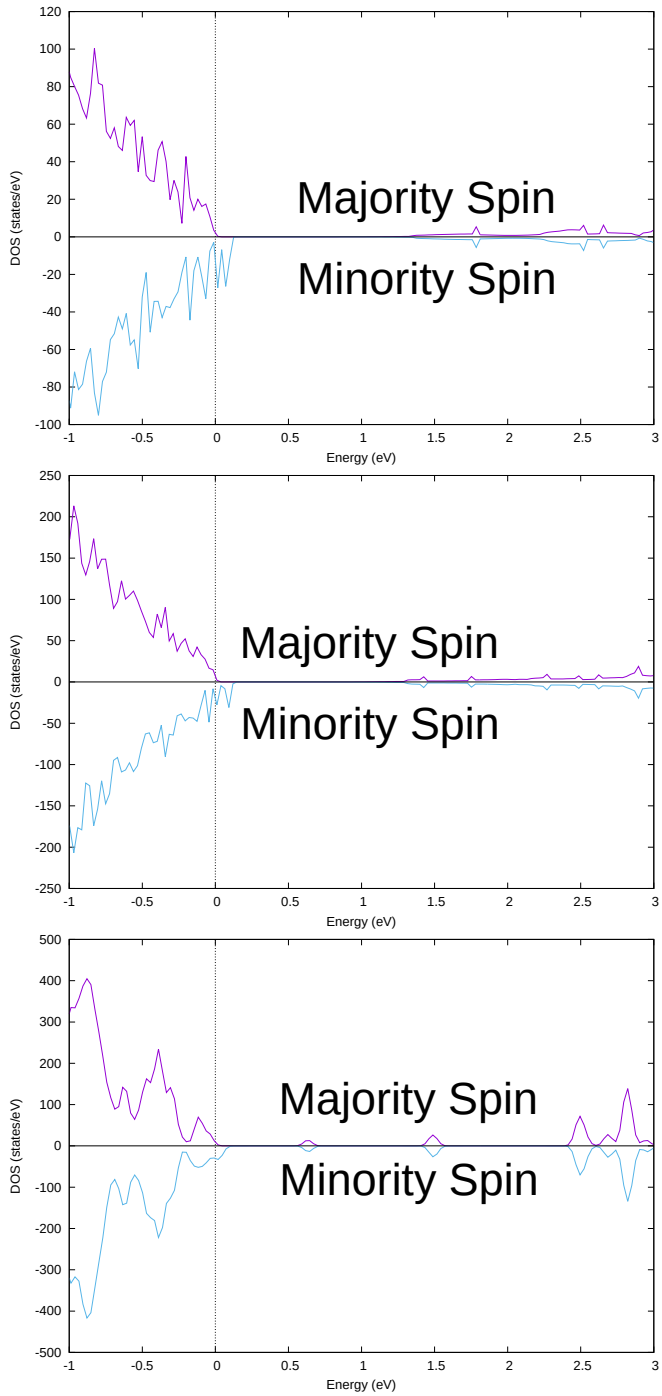

Figure 3.2: DOS of the single vacancy in ZnO 128-atoms supercell (upper part) and 512-atoms supercell (lower part). The Fermi level represents vertical grey line.

are expressed in Fig. 2.4).

We analyze the optimized of geometry structure in large supercell of ZnO in which the structure is C_{3v}. We find that the bond angles and atomic distances are slightly change in the large supercell: the bond angles, $\angle(\bar{1}\bar{1}\bar{1})$, are 116.2(116.9) and 116.0(117.0) for 256- and 512-atoms, respectively. These bond angles are found to be larger than the sp^3 hybridization angle.

Table 3.3: Optimized geometries of single cation vacancy in 256- and 512-atoms supercell of ZnO. The parameters: atomic distances (r_a and r_b) and bond angles ( ) are de ned in Figure 2.4. The average value of the three bond angles of the rst anion represents in Fig. 2.4.

Systems			r_a (Å)	r_b (Å)
256	116.2	116.9	3.647	3.592
512	116.0	117.0	3.661	3.617

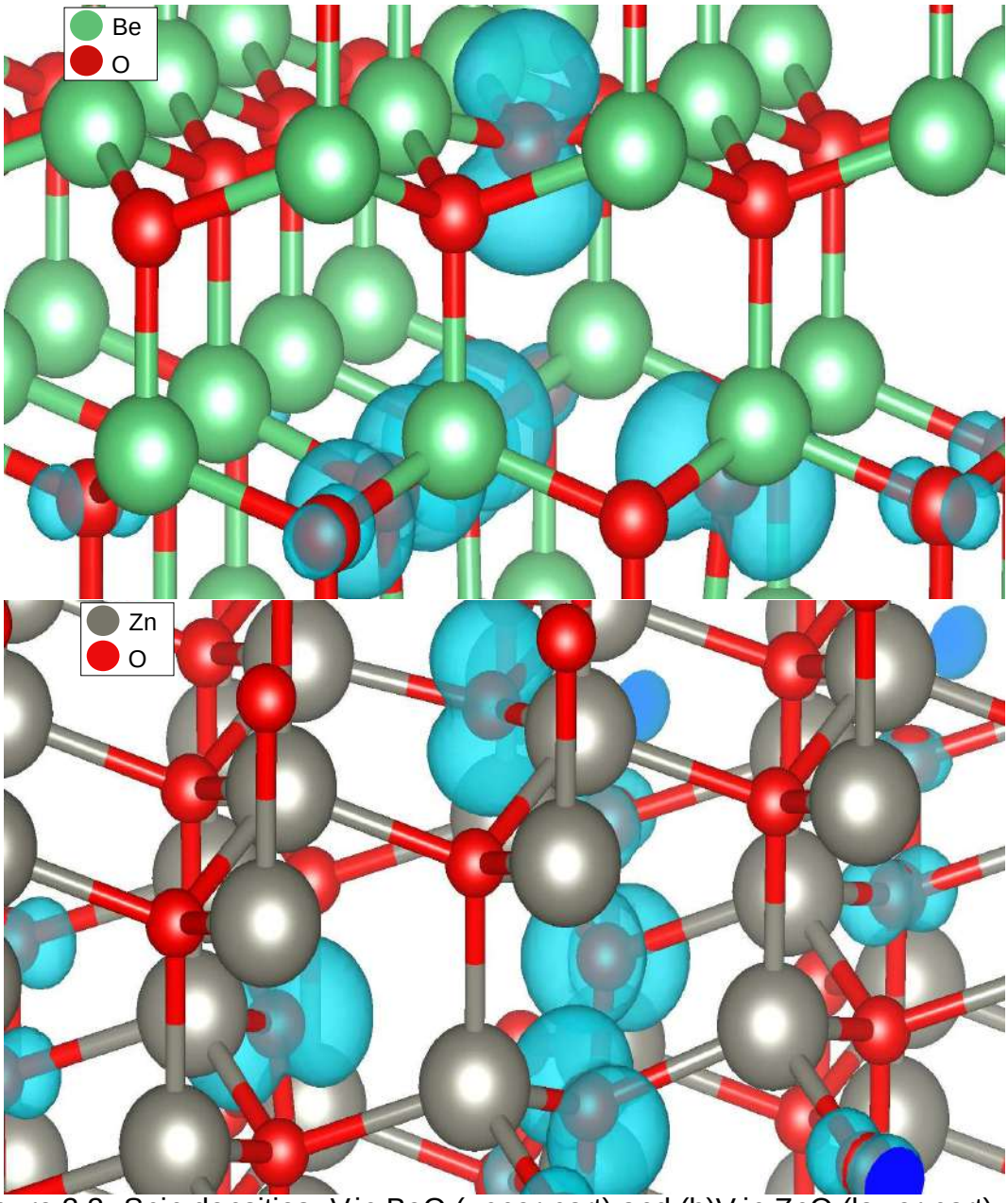

Figure 3.3: Spin densities: V_{Be} in BeO (upper part) and (b) V_{Zn} in ZnO (lower part). We set isovalues to be 10^{-3} electron/Å^3 and set its with cyan colors.

At the near four oxygen atoms in ZnO and BeO, the spin densities are found to be localized and mainly consist of the oxygen p orbitals and small s-component, as Figs. 3.1 and 3.3 shows. The small s-component can be

identi ed by analyzing the partial density of states (PDOS); the small s component is found at the defect E level of the minority spin (Fig.3.1). In fact, the small s-component is due to the bond angles of the near oxygen atoms is substantially larger than the sp^3 bond angle (109.5).

We next study cation vacancies in sul de semiconductors (ZnS and CdS). We nd that the stable structures are spin polarized C_{3v} symmetries as in the case of oxides. The calculate magnetic moments are 1.66 $_B$ (1.95 $_B$) for ZnS (CdS). The non-integer values are also found in this case because the nite dispersion of the defect t_1 and E levels as in the case of oxide (ZnO). In the past study, the non-integer values are also found[40, 41, 61].

We nd that at the near four sulfur atoms in sul des the bond angles are close to the sp^3 bond angle, as Table 2.2 shows. The bond angles ( ) of ZnS are 109.5 (110.5) and in the case of CdS are 114.2(113.1). The bond angles is close to the sp^3 bond angle due to the fact that the outward relaxation of the four sulfur atoms near vacancies are small. This e ect to the small atomic distance of sulfur-sulfur: the atomic distance, r_a (r_b), in ZnS is 1.1% (1.0%) larger than the ideal distance. Meanchile, the atomic distance of sulfur-sulfur in CdS, r_a (r_b), is 5.3% (2.3%) larger than the value of the ideal value (Table 2.2).

The spin density on the sul des semiconductors is localized at four near sulfur and contain more s-components since the bond angles are close to the sp^3 one, as shown in Fig.3.5. This is contrast with the oxides case that the s-components is small. We nd that the defect E level occupy by majority spin electrons contain large s component. As Figure of PDOS (Fig.3.4), the minority spin electrons of the defect E level have a large s-component than those in the case of oxides. The origin of the large s component is due to the bond angles of the near sulfur atoms are close to the sp^3 bond angle.

The spin polarization energy (E_p) is evaluated by measuring the energy of the non-magnetic state from the energy of the spin-polarized state

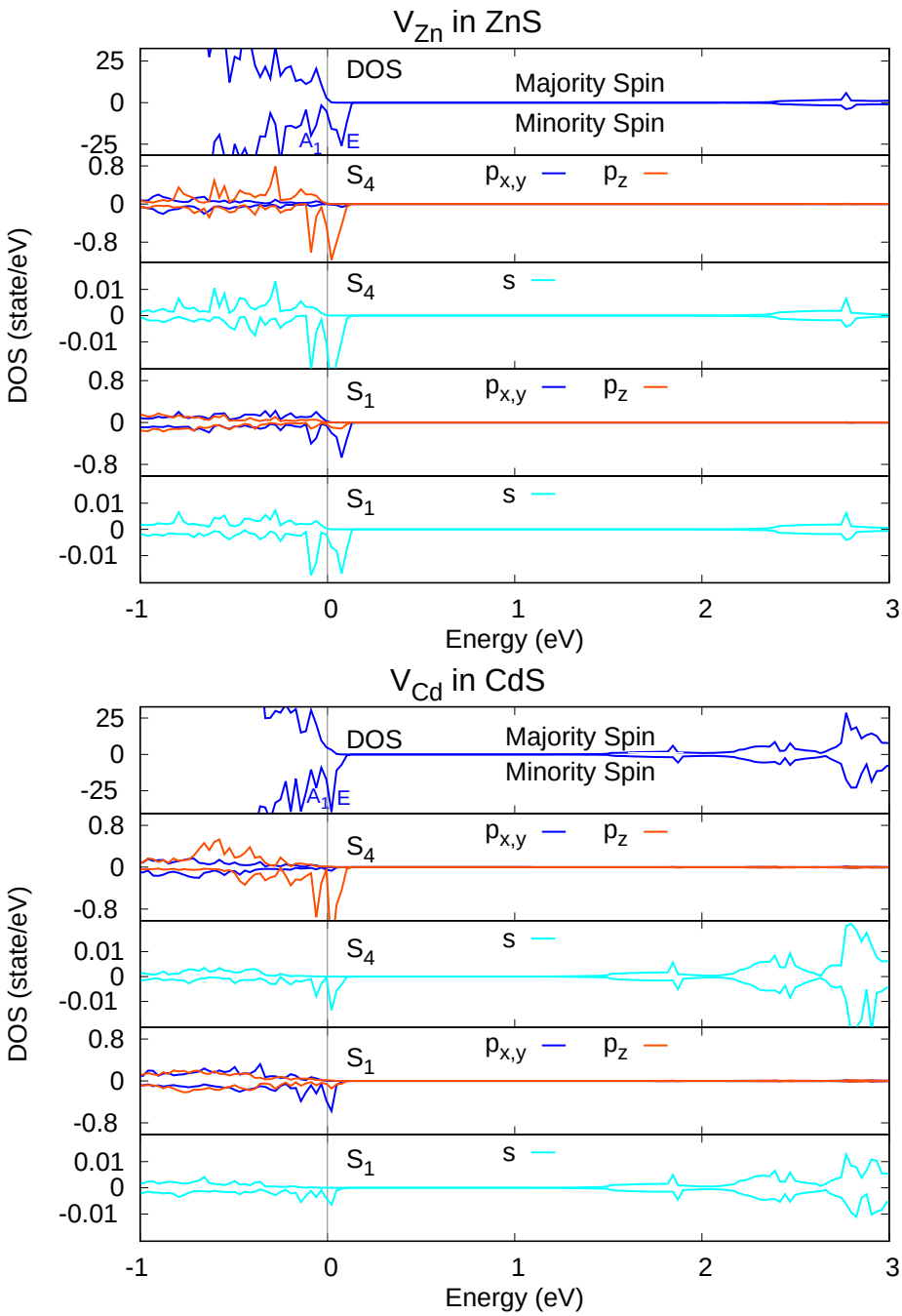

Figure 3.4: DOS and PDOS for the 1st and 4th atoms near cation vacancy in the case of BeO (upper part) and ZnO (lower part) which are de ned in Figure 2.4. The Fermi level represents vertical grey line.

Table 3.4: E_p (eV) is spin polarization energy and m($_B$) is the total magnetic moment for single cation vacancies in II-VI semiconductors.

Systems	E_p (eV)	m($_B$)
V_{Be} in BeO	0.35	2.00
V_{Zn} in ZnO	0.04	1.71
V_{Zn} in ZnS	< 0:01	1.66
V_{Cd} in CdS	< 0:01	1.95

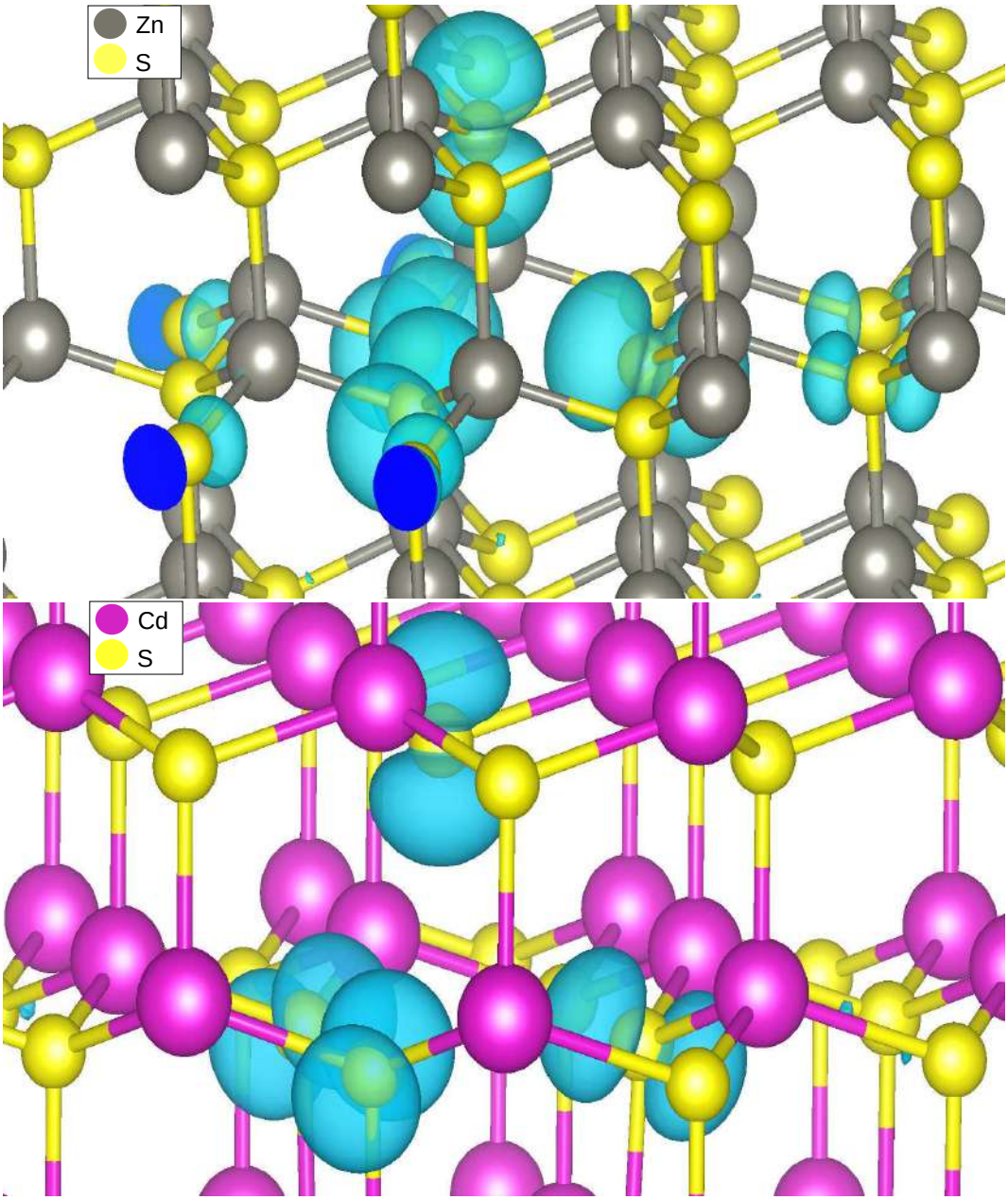

Figure 3.5: Spin densities: V_{Zn} in ZnS (upper part) and V_{Cd} in CdS (lower part). We set the isovalues to be 10^{-3} electron/Å^3 and set its with cyan colors.

(Table 3.4). We find that the calculation result of the E_p to be large in the case of oxides; the energy is 0.35 eV (0.04 eV) for BeO (ZnO), respectively. In contrast, the E_p of the sulfides are found to be small; the energy E_p are very small for ZnS and CdS, respectively, as Table 3.4 shows. We expect that the spin polarization energies E_p, are large in the case of oxides because the atomic radii of oxygen is much smaller than that of sulfur since the spin density is localized at the near four cation atoms. The small energies are also found in previous studies[33, 44]. Hence, the oxides are

good candidates for vacancy-induces spin-polarization materials.

3.4 Cation Vacancies in III-V Semiconductors

We next study cation vacancies in III-V semiconductors where the nitrides (BN, AlN, and GaN) and phosphides (GaP) semiconductors are examined. We first analyze nitrides semiconductors and find that the most stable structures are spin polarized C_{3v}. In the case of nitrides, we find that the magnetic moment is 3 $_B$: The defect E and A_1 levels are occupied (unoccupied) by three majority (minority) spin electrons as the DOS in Fig. 3.6 show; The E level splits into two peaks in the DOS. This is due to the artificial band dispersion of the supercell model; i.e., the E level is doubly degenerated at the point but splits into two at general k-points. These results are in sharp contrast with the results for II-VI semiconductors; The minority and majority spin electrons are occupied the defect A_1 level and the magnetic moment is 2 $_B$ in the case of II-VI semiconductors.

In the four nitrogen atoms near vacancies, the outward relaxations occur. As a result, the nitrogen-nitrogen distances r_a and r_b of BN (AlN) is 9.4% and 9.2% (11.6% and 11.1%) larger than the ideal distance of pristine wurtzite, we compare this bond lengths with ideal value as in Table 2.1 shows. We also find that the atomic distances in the case of GaN r_a and r_b are 9.2% and 9.4% larger than the ideal crystal, respectively (Table 2.1). In the nitrides case, at the four nitrogen atoms near the vacancies the bond angles are close to the sp^2 hybridization bond angle as is seen in Table 2.2: The bond angles( ) are 114.1 (114.1), 116.1 (117.4) and 115.0 (115.0) for BN, AlN, and GaN, respectively, as in Table 2.2 shows.

We analyze the spin density and find that at the near four nitrogen atoms is localized, as is shown in Fig. These spin densities are mainly consist of the p-orbitals of the nitrogen atoms and the small contributions of the s-orbitals from atoms near cation vacancies as is seen in Figs. 3.7. The small contribution of s-orbitals is due to the fact that the defect E and A_1 levels occupied (unoccupied) by majority (minority) spin contains p-

orbitals and the s-component is small. The defect E and A_1 levels show small s-components in Fig.3.6 of PDOS. In fact, the small s-components of the atoms near vacancies are due to the fact that the bond angles of the four near nitrogen atoms are substantially larger than the sp^3 bond angle (109.5).

We here also study the phosphide semiconductors (GaP). We compare phosphide and nitride semiconductors; we clarify the energetical stability of atom near cation vacancies in the two cases. First, GaP is formed in zinc blende structure[29] and recently the new study of GaP was observed that the wurtzite structure is achieved in the case of nanowires[62]. Since our purpose is to study the chemical trend for the anions in III-V semiconductors, the study of the bulk wurtzite GaP in is necessary. We also nd that the stable structure for cation vacancy in GaP is spin polarized state and the magnetic moment is found to be the same as those in nitride semiconductors. The moment magnetic moment in cation vacancy GaP is found to be 3 $_B$; by three majority (minority) spin electrons occupy the defect E and A_1 levels, as the Fig. 3.8 indicates. We observe the geometry structure and nd that the bond angle ( ) is 107.6 (107.4) for GaP and is thus close to the sp^3 bond angle (109.5) due to the fact small relaxation of the near four phosphorus atoms (Table2.2). The bond angle in GaP is close to the sp^3 bond angle because the outward relaxation is small and thus the atomic distance, r_a(r_b), is only 1.7% (5.5%) larger than the ideal crystal of GaP.

We nd that the spin density is localized at the four phosphide atoms near vacancies (Fig. 3.8). As the above mentioned, the bond angle in GaP is close to the sp^3 bond angle that makes the spin density contains more s-component compared to the case of nitrides (Figs.3.7 and 3.8). The spin density contains more s-component due to the fact that the defect E and A_1 levels contain more s-components than those of nitrides. We con rm that the spin density in GaP contain more s-components; The defect E and A_1 levels of the minority spin contain large s-components as the PDOS (Fig.

3.8) shows. The large s-component because the bond angles of the atoms near vacancies are closest to sp^3 bond angle.

Table 3.5: E_p (eV) is spin polarization energy and m ($_B$) is the total magnetic moment for single cation vacancies in III-V semiconductors.

Systems	E_p (eV)	m ($_B$)
V_B in BN	0.19	3.00
V_{Al} in AlN	0.83	3.00
V_{Ga} in GaN	0.48	3.00
V_{Ga} in GaP	< 0:01	3.00

We next evaluate the spin polarization energies E_p() of cation vacancies in nitrides and phospides. First, in nitride case, the energies for BN, AlN, and GaN are 0.19 eV, 0.83 eV and 0.48 eV, respectively. In the contrary, the small value of spin polarization energy is found in GaP case. We have analyzed the spin density of nitrides and phosphides in above mentioned. Since the spin densities are localized at the near four anions, we nd that the large values of spin polarization energies in nitrides are expected due to the fact that the nitrogen atom has a smaller atomic radii. The phosphorus atom have substantially large atomic radii than nitrogen and thus the spin polarization energy is found to be smaller than nitrides case. In previous study [33, 44], the spin polarization energy in GaP is smaller than GaN case. We conclude that the spin polarized state of the cation vacancy is stable in nitrides. In a previous section, we also concluded that the cation vacancy is stable in oxides. These conclusions are consistent with experimental results that high-temperature ferromagnetisms are found in cation vacancies of oxides and nitrides[24, 25, 22, 28, 30, 21].

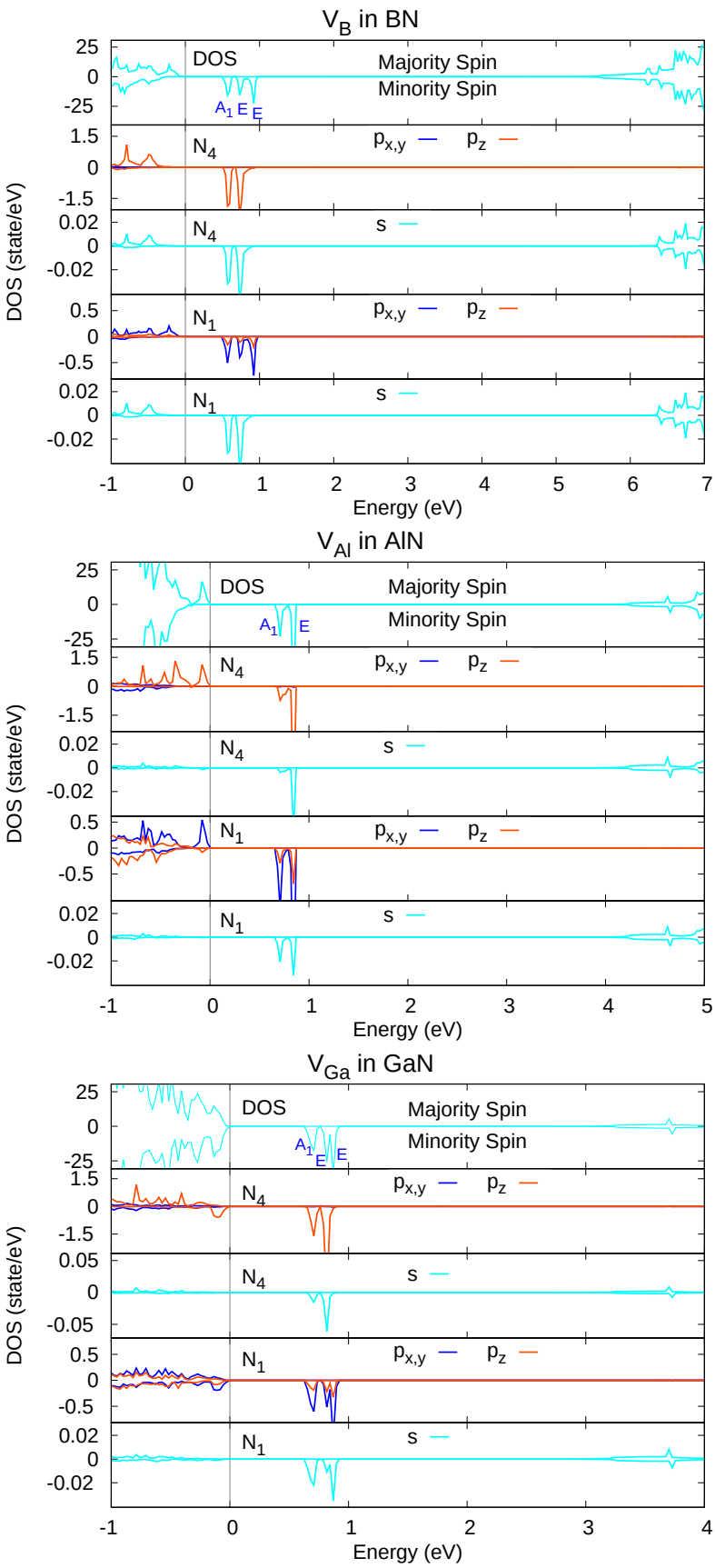

Figure 3.6: DOS and PDOS for the 1st and 4th of nitrogen atoms in the case of BN, AlN, and GaN (upper, middle, and lower part, respectively) which are de ned in Figure 2.4. The Fermi level represents vertical grey line.

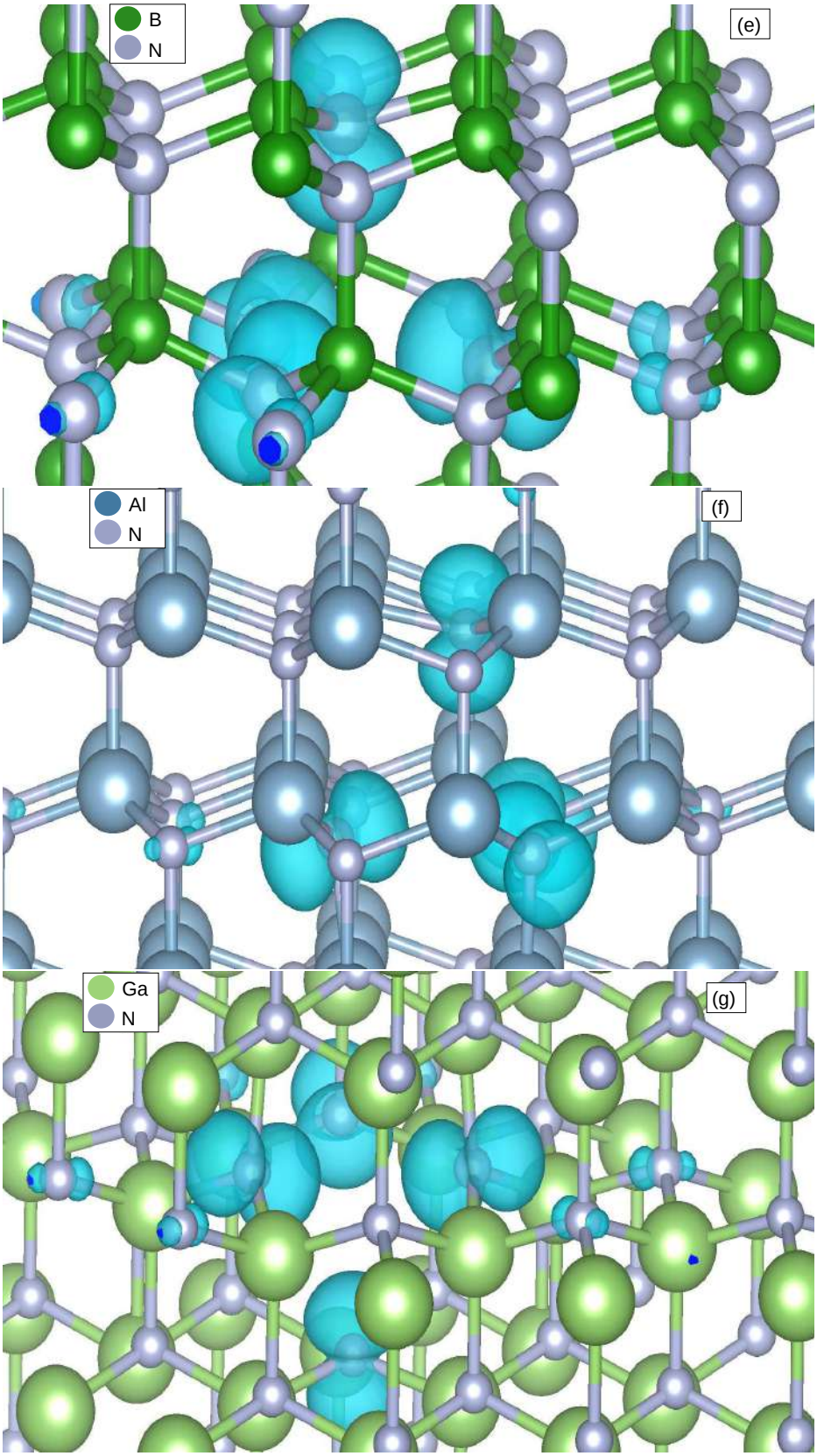

Figure 3.7: Spin densities: V_B in BN, V_{Al} in AlN, and V_{Ga} in GaN. We set the isovalues to be 10^{-3} electron/Å^3 and set its with cyan colors.

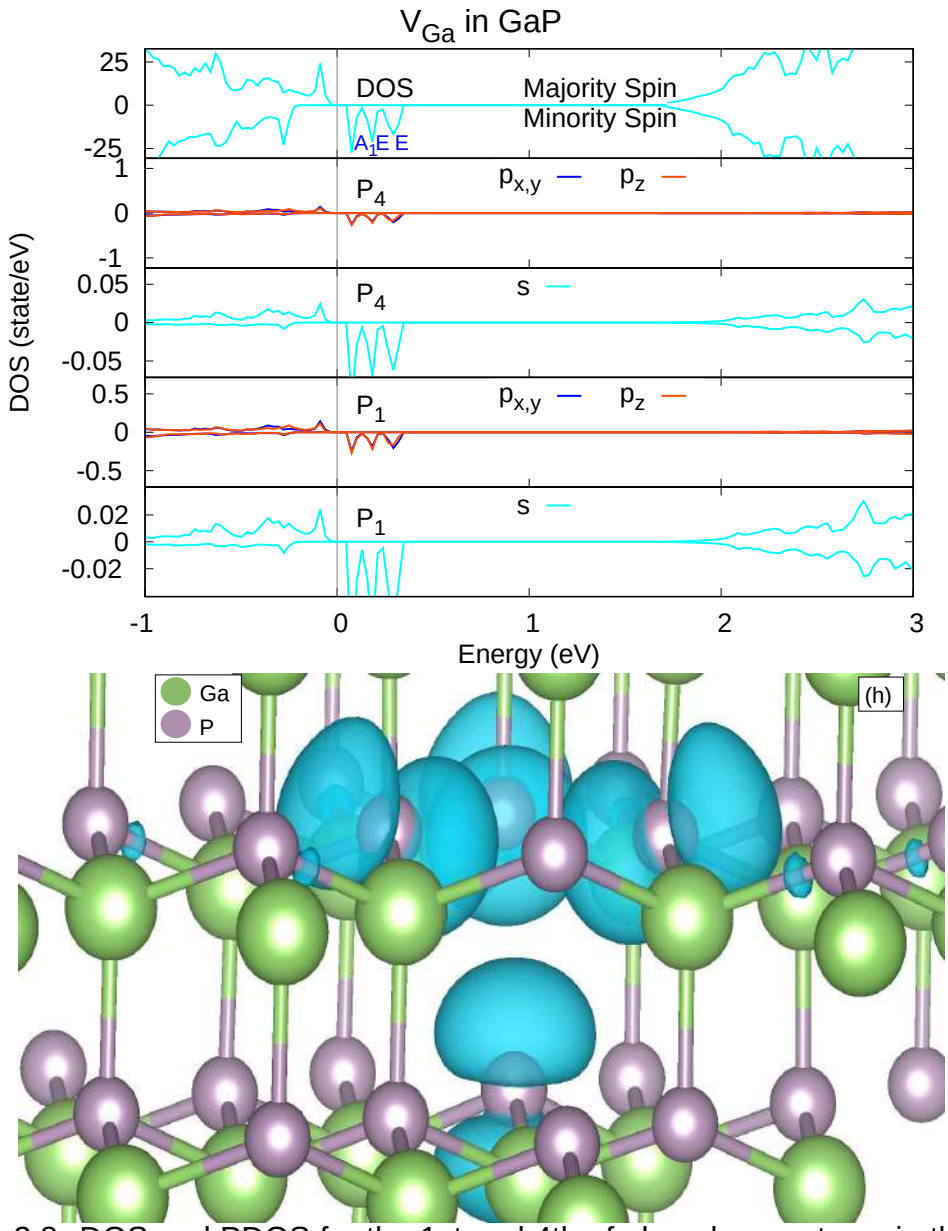

Figure 3.8: DOS and PDOS for the 1st and 4th of phosphorus atoms in the case of GaP (upper part) and spin densities (lower part). We set the isovalues to be 10^{-3} electron/Å^3 and set its with cyan colors.

Chapter 4

E ect of Symmetry Lowering

We have clari ed that the spin-polarized state are the most stable and the symmetry is C_{3v}, particularly, for cation vacancies in oxides and nitrides cases. The defect E level split when the symmetry of C_{3v} is lowered and thus the magnetic moments are expected to decrease. In the previous study, the Jahn-Teller distortion occurs in neutral single vacancy of group-IV (silicon)[64, 65, 66]. The energy of T_d level is occupied by two major-ity electron and the a_1 level is occupied by majority (minority) electron. Due to Jahn-Teller distortion, triply degenerate T_d level split into e and b_2 levels and majority (minority) spin is occupied. Therefore study of lower-ing symmetry in II-VI and III-V is necessary. In this chapter, we brief the e ect of symmetry lowering in the wurtzite structures.

4.1 E ect of Symmetry Lowering in II-VI Semiconduc-tors

We rst study the possibility of the occurrence of the symmetry lowering in case of oxides. We nd that In the case ZnO the stable structure is C_{3v} geometry and the defect E level is occupied by two majority spin electrons and thus the spin state is triplet (S=1). We nd that the Jahn-Teller (JT) e ect occurs and expects to lower the symmetry from C_{3v} to C_s. The de-fect E level splits into A' and A" and thus spin singlet (S=0) obtains on the system; The lower level of splits band (A' level) is occupied by two elec-

trons, as Fig.4.1 shows. We analyze that the pairing distortion occurs in the case of ZnO. The outward relaxation exists at the 4th atoms near vacancy and the inward relaxation appears in the 1st and 3rd atoms: the atomic distance, r_a, become small than atomic distance, r_b, as is illustrated in Fig. 4.2. Table 4.1 shows the symmetry lowering atomic geometries.

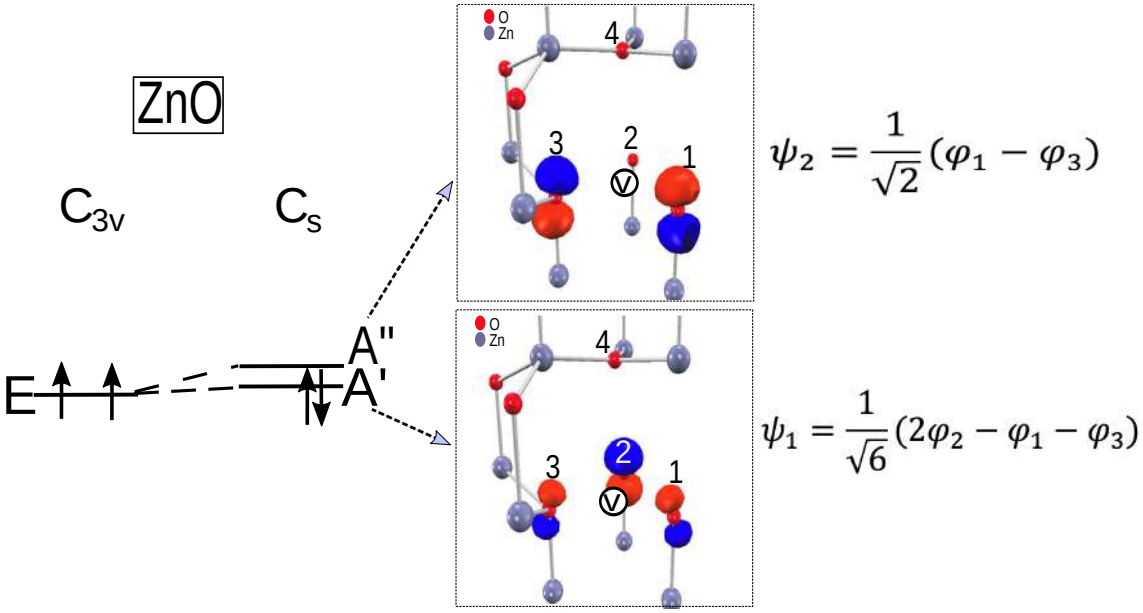

Figure 4.1: Energy diagram of the C_{3v} and C_s in the case of ZnO. The wavefunctions is represented as red (blue) colors indicates positive (negative) amplitudes.

Based on a simpli ed model, we here construct the wavefunctions to understand the mechanism of lowering symmetry. The wavefunctions consider by including the dangling bond orbitals, φ_i, of the four near anions (i=1-4) forming the tetrahedron; on the basal plane the three (i=1-3) anions dangling bond orbitals are located and 4th anion is located at the top of the tetrahedron (Fig.4.2). The E representation in the C_{3v} symmetry belong the two wavefunctions: $\psi_1 = \frac{1}{\sqrt{6}}(2\varphi'_2 - \varphi'_1 - \varphi'_3)$ and $\psi_2 = \frac{1}{\sqrt{2}}(\varphi'_1 - \varphi'_3)$. Due to the lowering symmetry to C_s, ψ_1 and ψ_2 belong to A' and A", respectively (Since φ'_4 belongs to A', it can be mixed with ψ_1 but the mixing is found to be very small as Fig. 4 shows). Since the lowering symmetry in ZnO case is pairing distortions, we nd that the A' level is lower than the A" level because the small distance between 1st and 3rd atoms (Fig. 4.2). The small splits between A' and A" is very small (0.01 meV). We con rm this energetical order by analyzing the wavefunctions obtained from the den-

sity functional calculation (Fig. 4.1). Since the pairing case change the geometries structures, the dirence between r_{a^0} and r_{b^0} is only 7 10 ^{3} Å (Table 4.1). The outward relaxation is weak because the JT is found to be very small. We also calculate and analyze the JT energy due to the pairing distortion: By measuring the energy of the low spin (spin singlet) C_{3v} symmetry to the energy of the low spin (spin singlet) C_s symmetry. We nd that the JT energy in ZnO is small (E_1 = 0:01 eV), as is seen in Table 4.1. Hence, the spin singlet C_s symmetry has 0.03 eV higher energy than the spin triplet state of the C_{3v} symmetry: we calculated as follow $E_2 = E_p E_1$ = 0:03 eV (Table 4.1).

We study the lowering symmetry in BeO case and nd that the depairing case occurs: the atomic distance r_{a^0} is larger than r_{b^0} (Fig.4.2). The defect E level splits into A' and A" as the same in ZnO case, but in depairing case the A' level is found to be higher than A" level. The energy of the symmetry lowering in depairing case BeO is very small (Table 4.1) and thus the spin triplet state of the C_{3v} symmetry is the most stable structure. In other case (ZnS and CdS), the symmetry lowering is found to be unstable. We conclude that the lowering symmetry in II-VI semiconductors is very weak and thus the most stable structure is spin triplet state of the C_{3v} symmetry.

Table 4.1: Calculated parameters of symmetry lowered atomic geometries. The atomic distances r_{a^0}, r_{b^0}, r_{c^0} and r_{d^0} are de ned in Figure 4.2. E_1 is the energy of the spin singlet (doublet) C_{3v} symmetry measured from the energy of the spin singlet (doublet) C_s symmetry in the case of II-VI (III-V) semiconductors. $E_2 = E_p E_1$ is the energy of the spin singlet (doublet) C_s symmetry measured from the energy of the spin triplet (quartet) C_{3v} symmetry in the case of II-VI (III-V) semiconductors.

Systems	type	r_{a^0} (Å)	r_{b^0} (Å)	r_{c^0} (Å)	r_{d^0} (Å)	E_1 (eV)	E_2 (eV)
V_{Zn} in ZnO	pairing	3.635	3.642	3.603	3.605	0.01	0.03
V_{Ga} in GaN	depairing	3.459	3.453	3.465	3.457	0.23	0.25
V_{Al} in AlN	depairing	3.550	3.549	3.482	3.481	< 0:01	0.83
V_{Be} in BeO	depairing	3.031	3.030	2.988	2.987	< 0:01	0.35

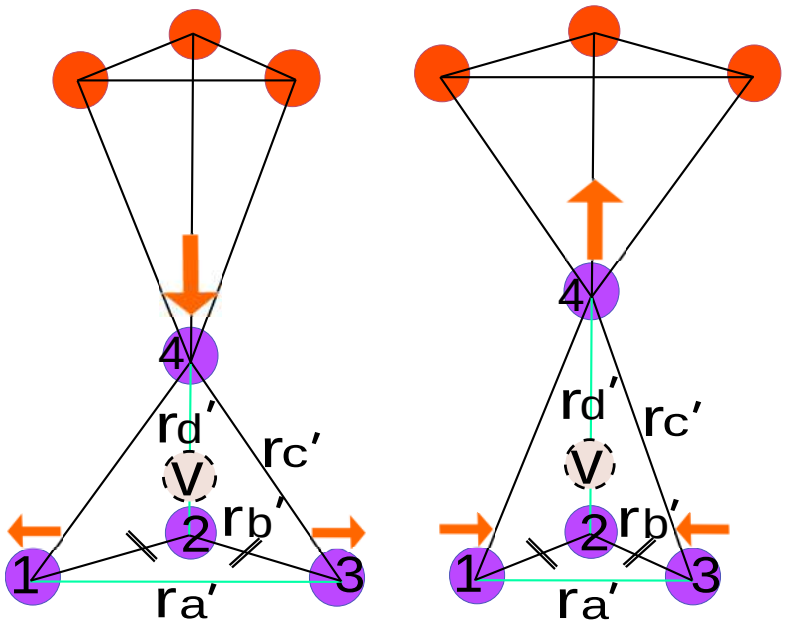

(a) Depairing (b) Pairing

Figure 4.2: Two kinds of symmetry lowering ect: (a) depairing and (b) pairing distortions.

4.2 E ect of Symmetry Lowering in III-V Semiconductors

The symmetry lowering in nitride semiconductors is also studied. As mention in previous section, in nitrides case, three majority electrons occupy the defect E and A_1 levels and thus the spin state is quartet ($S=3/2$). By analyzing of four-anion dangling model, we nd that on the A_1 level the wavefunction is expressed as $_3 = \frac{1}{\sqrt{3+\ ^2}}(' _1 + ' _2 + ' _3 \quad ' _4)$, where is a constant. As in the case of ZnO, the E level splits into A' ($_1$) and A" ($_2$) and A_1 ($_3$) becomes A' due to symmetry lowering from C_{3v} to C_s. In the case of GaN, we nd that depairing distortion occurs based on the result of the density functional calculation and this distortion makes the A" level is lower than the A' level, as is seen in Fig. 4.3. The origin of A' forms the A_1 level in the C_{3v} symmetry, which is this level has lower energy than the above two levels. We limit our calculation within the spin doublet ($S=1/2$) and nd that two electrons occupy the A' level and a single electron occupy in the A" level. The atomic distance between r_a and r_b is found to be small (0.006 Å) as in the case of ZnO. The ence between

r_{c^0} and r_{d^0} is 0.008 Åand this result is larger than that in ZnO case where in the ZnO case the dierence between r_{c^0} and r_{d^0} is 0.002 Å. (We de nd the r_{c^0} and r_{d^0} as in Fig. 4.2). The energy of the symmetry lowering (E_1) is 0.23 eV by measuring from the energy of the low spin (spin doublet) C_{3v} symmetry to the energy of the low spin (spin doublet) C_s symmetry. The energy in GaN is larger than than in ZnO case which the energy in ZnO is 0.01 eV. We calculate the dierence energy and nd that the spin doublet C_s state has 0.25 eV higher energy than that in the spin quartet C_{3v} state. In the GaN case, the spin quartet C_{3v} is found to be stable state because the spin-polarized energy (E_p) is large (0.48 eV), as seen in Table 4.1. We nd that in the both case ZnO and GaN the energies (E_1) inducing by the symmetry lowering and the values are found to be smaller than those of the spin-polarized energies (E_p). Therefore, the spin polarized C_{3v} state is the most stable state.

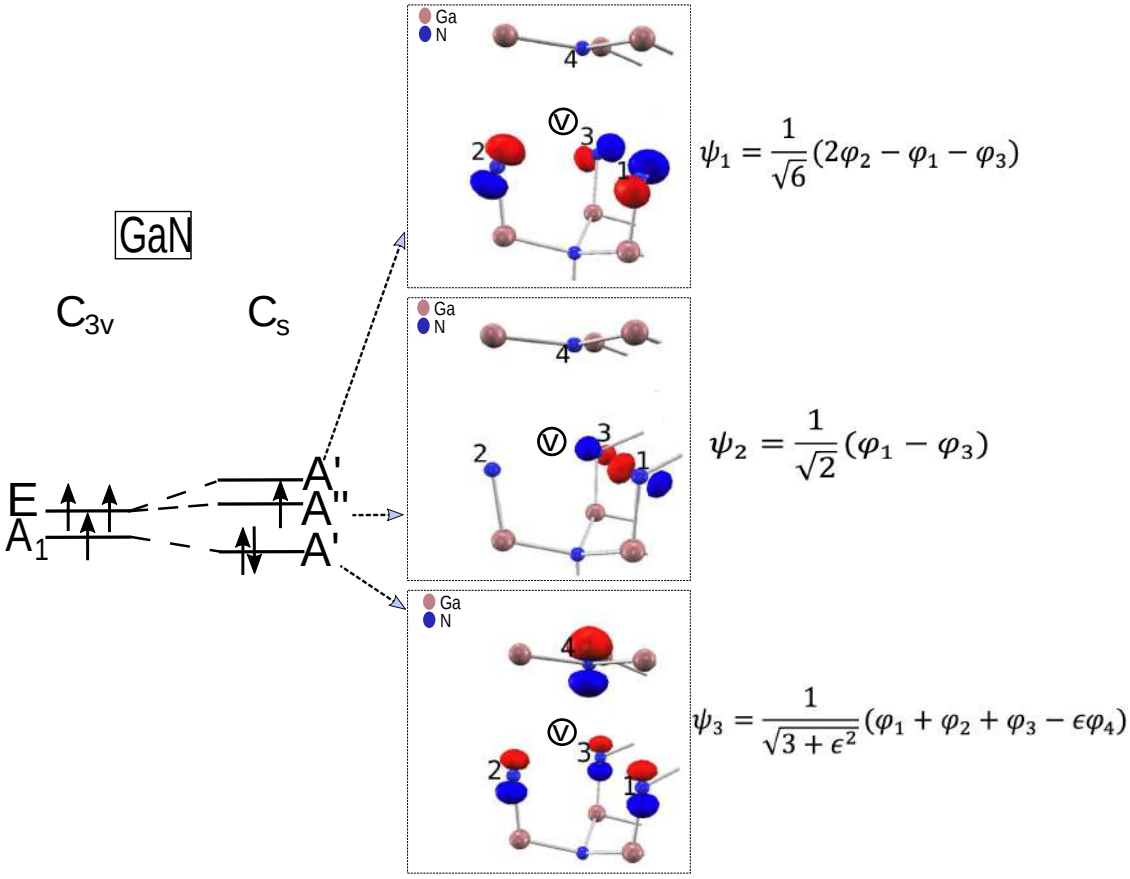

Figure 4.3: Energy diagram of the C_{3v} and C_s in the case of GaN. The wavefunctions is represented as red (blue) colors indicates positive (negative) amplitudes.

We also study the symmetry lowering eect in other III-V semicon-

ductors (BN, AlN, adn GaP). We nd that the depairing distortion and the energy of the symmetry lowering are very small in the case AlN (4.1). The spin quartet state of C_{3v} geometry has much lower energy than the spin doublet state of the doublet C_s geometry, as in Table 4.1. In the III-V case, we do not detect the pairing case as in the case of oxides. We study the symmetry lowering in the BN and GaP case and nd the unstable state.

We have studied the symmetry lowering eect in cation vacancies of II-VI and III-V semiconductors and found that the symmetry lowering e ect is very small. We nd two types of lowering symmetry: pairing and depairing distortions, in which atomic distance between rst and third atoms in pairing distortion becoming close and vice versa, as is illustrated in Fig4.2[63]. The metastable or unstable state are found in the spin singlet (doublet) C_s geometries and thus the most stable structures in the case II-VI (III-V) semiconductors are triplet (quartet) C_{3v} Symmetries. Our result are in sharp contrast with the case of of silicon neutral monovacancy[64, 65, 66]. In the Silicon monovacancy, the inward ralaxation occurs at the four nearest Si atoms and the interactions between Si atoms become large. As a result, the spin singlet state become the most stable state because the JT distortion inducing the bonding of the dangling bonds.

Chapter 5

Conclusion

5.1 Summary

We have carried out spin-polarized DFT calculations of cation vacancies in II-VI (oxides and sul des) and III-V (nitrides and phosphides) wurtzite structure semiconductors. The most stable structures in II-VI and III-V semiconductors are C_{3v} symmetries and are spin-polarized. The structures are stable when the k-point is gradually increased since the bond angles and bond lengths are well convergence We nd that in II-VI semiconductors two majority (minority) spin electrons occupy (unoccupy) defect E level lead to the magnetic moment $2\mu_B$. On the contrary, three majority spin electrons occupy the defect E and A_1 levels in III-V semiconductors and three minority spin electrons unoccupy. In the case of oxides and nitrides semiconductors, the spin polarization energies are found to be larger than other semiconductors: the semiconductors consisting of rst-row anions, i.e., oxygen and nitrogen atoms. This large spin polarization energies are due to the atomic radii smaller than the other semiconductors cause te large outward relaxation of atoms near vacancies. We have studied the possibility of the symmetry lowering distortion and found that the structures shift to lower symmetries from C_{3v} to C_s. We have found that two types distortions due to lowering symmetry: pairing and depairing distortions. These lowering symmetries are found to leads spin multiplicity and the energies are higher than the spin-polarized state. Therefore, we conclude that

the spin-polarized C_{3v} symmetry is the most stable structures.

5.2 Future Scope

We have studied the mechanism of spin-polarized in cation vacancies in II-VI and III-V semiconductors based on density functional theory. We have found that the most stable structures are spin-polarized C_{3v} symmetry and large spin-polarization energies are found in the oxides and nitrides semiconductors. Therefore, the best materials to use in ferromagnetic semiconductors are expected from oxides and nitrides.

The antiferromagentics in wurtzite dilute magnetic semiconductors have been observed. In the several cases, the antiferromagnetic states are theoretically studied by using two apart vacancies. The energy of antispin-polarized is found to be small in the nitrides and oxides semiconductors and the spin-polarized is found to be the most stable. We expect that the distance of the two vacancies effects the polarization. When the distance between the two vacancies is close, we expect that the possibility of the ground state is the spin-polarized state. The antispin-polarized was study by positron annihilation study and was existed in oxide cases[67, 68, 69, 70]. Study the antispin-polarized will support the understanding of polarization in semiconductors.

Appendix A

Character Tables

In Chapter 2 and 3, we mentioned the con guration of a pristine and single cation vacancy in II-VI and III-V semiconductors having the C_{6v} and C_{3v}, respectively. We use group theory to analyze the symmetries. In this part, we explain the symmetry and group theory. We use Mulliken symbol for conventional irreducible representations.

Table A.1: Character table of C_{6v}. The form of pristine wurtzite is C_{6v} symmetry.

C_{6v}	E	$2C_6$	$2C_3$	C_2	3_v	3_d
A_1	1	1	1	1	1	1
A_2	1	1	1	1	-1	-1
B_1	1	-1	1	-1	1	-1
B_2	1	-1	1	-1	-1	1
E_1	2	1	-1	-2	0	0
E_2	2	-1	-1	2	0	0

Table A.2: Character table of C_{3v} symmetry. The form of a single vacancy in wurtzite is C_{3v} symmetry.

C_{3v}	E	$2C_3$	3_v
A_1	1	1	1
A_2	1	1	-1
E	2	-1	0

Appendix B

Wavefunctions

We model the wavefunctions of near four-anions (i=1-4) forming the tetrahedron by using simple model which includes dangling bond orbitals, p_i. Three (i=1-3) anions are located on the basal plane and the fourth atom is located at the top of the tetrahedron, as is seen in Fig.2.4. The wavefunctions are analyzed at the point at the first Brillouin zone.

We first construct the character table of C_{3v} as the Table B.1 and illustrate the four-anions near vacancy as the Fig.B.1. We symbolize the four-anions as: Three anions a_1, a_2, a_3 and fourth anions a_4, respectively. C_{3v} have two three symmetry operation (rotation by and 2). C_3 and C_3^2 are rotation under and 2 , respectively. $_{vi}$ is reflection in a vertical plane and C_{3v} have three reflections as $_{v1}$, $_{v2}$ and $_{v3}$, respectively.

First, let a_1, a_2, a_3 as a identity E, as Table B.1 shows. We first consider a_1. We rotate a_1 by (C_3) and find a_1 become a_2, as is shown in Table B.1. We rotate again a_1 by 2 (C_3^2) and get a_1 become a_3. The vertical reflection of a_1 to the $_{v1}$ is a_1 itself, so we get a_1. The reflection of $_{v2}$ and $_{v3}$ are a_2 and a_3, respectively, as is seen in Table B.1. Then, we multiply a_1 by the irreducible representation of A_1 in C_{3v} and the result are added to get the wavefunction of A_1, as follow:

$$
\begin{aligned}
A_1 &= a_1 + a_2 + a_3 + a_1 + a_2 + a_3 \\
&= 2a_1 + 2a_2 + 2a_3 \\
A_1 &= a_1 + a_2 + a_3; \qquad \text{(B.1)}
\end{aligned}
$$

Table B.1: Character table of C_{3v} symmetry. The form of a single vacancy in wurtzite is C_{3v} symmetry.

C_{3v}	E	C_3	C_3^2	$_{v1}$	$_{v2}$	$_{v3}$
A_1	1	1	1	1	1	1
A_2	1	1	1	-1	-1	-1
E	2	-1	-1	0	0	0
a_1	a_1	a_2	a_3	a_1	a_2	a_3
a_2	a_2	a_3	a_1	a_3	a_1	a_2
a_3	a_3	a_1	a_2	a_2	a_3	a_1

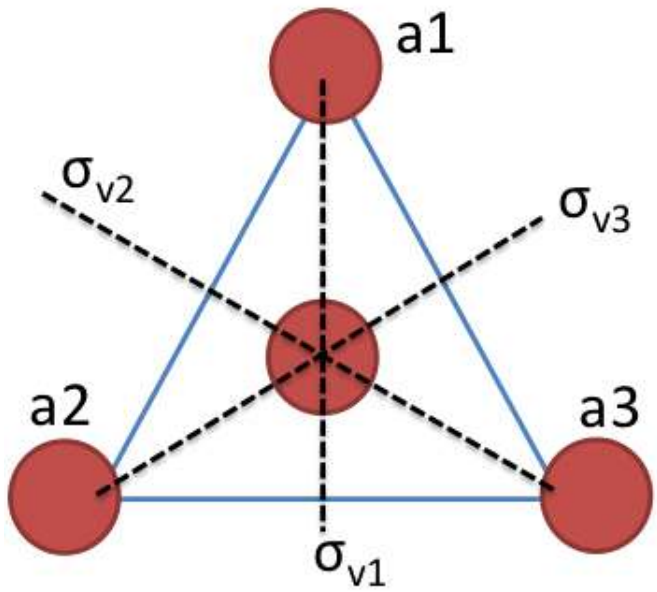

Figure B.1: Illustration of bond in C_{3v}. $_x$ represents the mirror translation.

We do the same with a_2 and a_3, as in Table B.1. Since the irreducible representation E has two kinds of the wavefunction, we construct the wavefunction by solving two equations. The rst wavefunction is from a_2, the direct multiply by the irreducible representation of E, as follow:

$$E = 2a_2 \quad a_3 \quad a_1; \tag{B.2}$$

The second wavefunction is by solving a_1 and a_3 and we get :

$$E = a_1 \quad a_3: \tag{B.3}$$

The above solution is to construct the wavefunctions of A_1 and E, then

we can get the dangling bond orbitals, by changing the a_1; a_2; a_3 to $'_1$; $'_2$; $'_3$. We consider the wavefunctions in three atoms: $_1 = \frac{1}{\sqrt{6}}(2'_2 \quad '_1 \quad '_3)$ and $_2 = \frac{1}{\sqrt{2}}('_1 \quad '_3)$. Three atoms and fourth atoms: $_3 = \frac{1}{\sqrt{3+\ ^2}}('_1 + '_2 + '_3 \quad '_4)$.

Bibliography

[1] I. M. Ross. The invention of the transistor. *Proceedings of the IEEE*, 86(1):7–28, 1998.

[2] Wu Jerry, Shen Yin-Lin, Reinhardt Kitt, Szu Harold, and Dong Boqun. A nanotechnology enhancement to moore's law. *Applied Computational Intelligence and Soft Computing*, 2013, Jan 2013.

[3] M. N. Baibich, J. M. Broto, A. Fert, F. Nguyen Van Dau, F. Petroff, P. Etienne, G. Creuzet, A. Friederich, and J. Chazelas. Giant magnetoresistance of (001)fe/(001)cr magnetic superlattices. *Phys. Rev. Lett.*, 61:2472–2475, Nov 1988.

[4] G. Binasch, P. Grünberg, F. Saurenbach, and W. Zinn. Enhanced magnetoresistance in layered magnetic structures with antiferromagnetic interlayer exchange. *Phys. Rev. B*, 39:4828–4830, Mar 1989.

[5] T. Dietl, H. Ohno, F. Matsukura, J. Cibert, and D. Ferrand. Zener model description of ferromagnetism in zinc-blende magnetic semiconductors. *Science*, 287(5455):1019–1022, 2000.

[6] H. Ohno. Bridging semiconductor and magnetism. *Journal of Applied Physics*, 113(13):136509, 2013.

[7] Tomasz Dietl. Interplay between carrier localization and magnetism in diluted magnetic and ferromagnetic semiconductors. *Journal of the Physical Society of Japan*, 77(3):031005, 2008.

[8] H. Ohno. Making nonmagnetic semiconductors ferromagnetic. *Science*, 281(5379):951–956, 1998.

[9] J.M.D. Coey. Dilute magnetic oxides. Current Opinion in Solid State and Materials Science, 10(2):83 – 92, 2006.

[10] Zhi Ren Xiao, Guang Yu Guo, Po Han Lee, Hua Shu Hsu, and Jung Chun Andrew Huang. Oxygen vacancy induced ferromagnetism in v2o5-x. Journal of the Physical Society of Japan, 77(2):023706, 2008.

[11] T. Schallenberg and H. Munekata. Preparation of ferromagnetic (in,mn)as with a high curie temperature of 90k. Applied Physics Letters, 89(4):042507, 2006.

[12] M. Wang, R. P. Campion, A. W. Rushforth, K. W. Edmonds, C. T. Foxon, and B. L. Gallagher. Achieving high curie temperature in (ga,mn)as. Applied Physics Letters, 93(13):132103, 2008.

[13] V. Novák, K. Olejník, J. Wunderlich, M. Cukr, K. Výborný, A. W. Rushforth, K. W. Edmonds, R. P. Campion, B. L. Gallagher, Jairo Sinova, and T. Jungwirth. Curie point singularity in the temperature derivative of resistivity in (ga,mn)as. Phys. Rev. Lett., 101:077201, Aug 2008.

[14] J. M. D. Coey, M. Venkatesan, P. Stamenov, C. B. Fitzgerald, and L. S. Dorneles. Magnetism in hafnium dioxide. Phys. Rev. B, 72:024450, Jul 2005.

[15] Keith P. McKenna and David Muñoz Ramo. Electronic and magnetic properties of the cation vacancy defect in hfo_2. Phys. Rev. B, 92:205124, Nov 2015.

[16] M. Venkatesan, J. M. D. Coey, and C. B. Fitzgerald. Unexpected magnetism in a dielectric oxide. Nature, 430:630, 2004.

[17] Chaitanya Das Pemmaraju and S. Sanvito. Ferromagnetism driven by intrinsic point defects in hfo_2. Phys. Rev. Lett., 94:217205, Jun 2005.

[18] Nguyen Hoa Hong, Joe Sakai, Nathalie Poirot, and Virginie Brizé. Room-temperature ferromagnetism observed in undoped semiconducting and insulating oxide thin films. Phys. Rev. B, 73:132404, Apr 2006.

[19] J. Osorio-Guillén, S. Lany, S. V. Barabash, and A. Zunger. Nonstoichiometry as a source of magnetism in otherwise nonmagnetic oxides: Magnetically interacting cation vacancies and their percolation. Phys. Rev. B, 75:184421, May 2007.

[20] Yu Liu, Liangbao Jiang, Gang Wang, Sibin Zuo, Wenjun Wang, and Xiaolong Chen. Adjustable nitrogen-vacancy induced magnetism in aln. Applied Physics Letters, 100(12):122401, 2012.

[21] Pratibha Dev, Yu Xue, and Peihong Zhang. Defect-induced intrinsic magnetism in wide-gap iii nitrides. Phys. Rev. Lett., 100:117204, Mar 2008.

[22] C. Madhu, A. Sundaresan, and C. N. R. Rao. Room-temperature ferromagnetism in undoped GaN and CdS semiconductor nanoparticles. Phys. Rev. B, 77:201306, May 2008.

[23] Nguyen Hoa Hong, Nathalie Poirot, and Joe Sakai. Ferromagnetism observed in pristine SnO_2 thin films. Phys. Rev. B, 77:033205, Jan 2008.

[24] K. Potzger, Shengqiang Zhou, J. Grenzer, M. Helm, and J. Fassbender. An easy mechanical way to create ferromagnetic defective zno. Applied Physics Letters, 92(18):182504, 2008.

[25] S. M. Evans, N. C. Giles, L. E. Halliburton, and L. A. Kappers. Further characterization of oxygen vacancies and zinc vacancies in electron-irradiated zno. Journal of Applied Physics, 103(4):043710, 2008.

[26] Daqiang Gao, Jing Zhang, Jingyi Zhu, Jing Qi, Zhaohui Zhang, Wenbo Sui, Huigang Shi, and Desheng Xue. I. vacancy-mediated

magnetism in pure copper oxide nanoparticles. Nanoscale Research Letters, 5:769–772, 2010.

[27] A. Droghetti, C. D. Pemmaraju, and S. Sanvito. Polaronic distortion and vacancy-induced magnetism in mgo. Phys. Rev. B, 81:092403, Mar 2010.

[28] Masaki Maekawa, Seiji Sakai, Atsumi Miyashita, and Atsuo Kawasuso. Spin-polarized positron annihilation measurement on ga vacancies in p-type gane. e-Journal of Surface Science and Nanotechnology, 16:347–350, 2018.

[29] T. A. Kennedy, N. D. Wilsey, J. J. Krebs, and G. H. Stauss. Electronic spin of the ga vacancy in gap. Phys. Rev. Lett., 50:1281–1284, Apr 1983.

[30] Masaki Maekawa, Hiroshi Abe, Atsumi Miyashita, Seiji Sakai, Shunya Yamamoto, and Atsuo Kawasuso. Vacancy-induced ferromagnetism in zno probed by spin-polarized positron annihilation spectroscopy. Applied Physics Letters, 110(17):172402, 2017.

[31] Qian Wang, Qiang Sun, Gang Chen, Yoshiyuki Kawazoe, and Puru Jena. Vacancy-induced magnetism in zno thin lms and nanowires. Phys. Rev. B, 77:205411, May 2008.

[32] Dongyoo Kim, Jeong-hwa Yang, and Jisang Hong. Ferromagnetism induced by zn vacancy defect and lattice distortion in zno. Journal of Applied Physics, 106(1):013908, 2009.

[33] O. Volnianska and P. Boguslawski. High-spin states of cation vacancies in gap, gan, aln, bn, zno, and beo: A rst-principles study. Phys. Rev. B, 83:205205, May 2011.

[34] D. Galland and A. Herve. Esr spectra of the zinc vacancy in zno. Physics Letters A, 33(1):1 – 2, 1970.

[35] Guoxing Zhu, Shuguang Zhang, Zheng Xu, Jing Ma, and Xiaoping Shen. Ultrathin zns single crystal nanowires: Controlled synthesis and room-temperature ferromagnetism properties. Journal of the American Chemical Society, 133(39):15605–15612, 2011. PMID: 21870837.

[36] Donglin Guo, Hao Hua, Qi Yang, Xiaoyan Li, and Chenguo Hu. Magnetism in dopant-free hexagonal cds nanorods: Experiments and rst-principles analysis. The Journal of Physical Chemistry, C 118(21):11426–11431, 2014.

[37] I. S. El mov, S. Yunoki, and G. A. Sawatzky. Possible path to a new class of ferromagnetic and half-metallic ferromagnetic materials. Phys. Rev. Lett., 89:216403, Nov 2002.

[38] Hongxia Wang, Zhaocun Zong, and Yu Yan. Mechanism of multi-defect induced ferromagnetism in undoped rutile TiO_2. Journal of Applied Physics, 115(23):233909, 2014.

[39] Na Hong Song, Yu Sheng Wang, Li Ying Zhang, Yu Ye Yang, and Yu Jia. Density functional theory study of tunable electronic and magnetic properties of monolayer beo with intrinsic vacancy and transition metal substitutional doping. Journal of Magnetism and Magnetic Materials, 468:252 – 258, 2018.

[40] Wen-Zhi Xiao, Ling-ling Wang, Qing-Yan Rong, Gang Xiao, and Bo Meng. Magnetism in undoped zns studied from density functional theory. Journal of Applied Physics, 115(21):213905, 2014.

[41] T. Chanier, I. Opahle, M. Sargolzaei, R. Hayn, and M. Lannoo. Magnetic state around cation vacancies in ii–vi semiconductors. Phys. Rev. Lett., 100:026405, Jan 2008.

[42] Xiaopeng Wang, Mingwen Zhao, Tao He, Zhenhai Wang, and Xiangdong Liu. Can cation vacancy defects induce room temperature

ferromagnetism in gan? Applied Physics Letters, 102(6):062411, 2013.

[43] O. Volnianska and P. Boguslawski. Local and collective magnetism of gallium vacancies in gan studied by gga+u approach. Journal of Magnetism and Magnetic Materials, 401:310 – 319, 2016.

[44] O Volnianska and P Boguslawski. Magnetism of solids resulting from spin polarization of p orbitals. Journal of Physics: Condensed Matter, 22(7):073202, feb 2010.

[45] Pierre Hohenberg and Walter Kohn. Inhomogeneous electron gas. Physical review, 136(3B):B864, 1964.

[46] Walter Kohn and Lu Jeu Sham. Self-consistent equations including exchange and correlation effects. Physical review, 140(4A):A1133, 1965.

[47] John P Perdew and Alex Zunger. Self-interaction correction to density-functional approximations for many-electron systems. Physical Review B, 23(10):5048, 1981.

[48] John P Perdew and Yue Wang. Accurate and simple analytic representation of the electron-gas correlation energy. Physical Review B, 45(23):13244, 1992.

[49] John P Perdew, Kieron Burke, and Matthias Ernzerhof. Generalized gradient approximation made simple. Physical review letters, 77(18):3865, 1996.

[50] U von Barth and L Hedin. A local exchange-correlation potential for the spin polarized case. i. Journal of Physics C: Solid State Physics, 5(13):1629–1642, jul 1972.

[51] J Grotendorst, S. Blügel, and D. (Eds.) Marx. Computational Nanoscience: Do It Yourself!, volume 31. John von Neumann Institute for Computing, Jülich, 2006.

[52] Christoph R. Jacob and Markus Reiher. Spin in density-functional theory. International Journal of Quantum Chemistry, 112(23):3661–3684, 2012.

[53] Volker Heine. Group theory in quantum mechanics: an introduction to its present usage. Courier Corporation, 2007.

[54] Mildred S Dresselhaus, Gene Dresselhaus, and Ado Jorio. Group theory: application to the physics of condensed matter. Springer Science & Business Media, 2007.

[55] Susumu Minami, Itaru Sugita, Ryosuke Tomita, Hiroyuki Oshima, and Mineo Saito. Group-theoretical analysis of two-dimensional hexagonal materials. Japanese Journal of Applied Physics, 56(10):105102, sep 2017.

[56] Nuning Anugrah Putri Namari and Mineo Saito. Electronic band structures of group-v two-dimensional materials. Japanese Journal of Applied Physics, 58(6):061003, may 2019.

[57] A ah Zaharo, Acep Purqon, Toto Winata, and Mineo Saito. Electronic structure of puckered group IV–VI two-dimensional monolayer materials. Japanese Journal of Applied Physics, 59(7):071006, jun 2020.

[58] Muhammad Yusuf Hakim Widianto, Hana Pratiwi Kadarisman, Amran Mahfudh Yatmeidhy, and Mineo Saito. Spin-polarized cation monovacancies in wurtzite structure semiconductors: rst-principles study. Japanese Journal of Applied Physics, 59(7):071001, jun 2020.

[59] http://azuma.nims.go.jp/cms .

[60] Haowei Peng, H. J. Xiang, Su-Huai Wei, Shu-Shen Li, Jian-Bai Xia, and Jingbo Li. Origin and enhancement of hole-induced ferromagnetism in rst-row d^0 semiconductors. Phys. Rev. Lett., 102:017201, Jan 2009.

[61] Jian-Ping Tang, Ling ling Wang, Hai-Jun Luo, and Wen-Zhi Xiao. Magnetic properties in zinc-blende cds induced by cd vacancies. Physics Letters A, 377(7):572 – 576, 2013.

[62] S. Assali, I. Zardo, S. Plissard, D. Kriegner, M. A. Verheijen, G. Bauer, A. Meijerink, A. Belabbes, F. Bechstedt, J. E. M. Haverkort, and E. P. A. M. Bakkers. Direct band gap wurtzite gallium phosphide nanowires. Nano Letters, 13(4):1559–1563, 2013. PMID: 23464761.

[63] Muhammad Yusuf Hakim Widianto, Hana Pratiwi Kadarisman, Amran Mahfudh Yatmeidhy, and Mineo Saito. Spin-polarized cation monovacancies in wurtzite structure semiconductors: rst-principles study. Japanese Journal of Applied Physics, 59(7):071001, jun 2020.

[64] Mineo Saito, Atsushi Oshiyama, and Shoichiro Tanigawa. Anisotropic momentum distribution of positron-annihilation radiation in semiconductors. Phys. Rev. B, 44:10601–10609, Nov 1991.

[65] Osamu Sugino and Atsushi Oshiyama. Vacancy in si: Successful description within the local-density approximation. Phys. Rev. Lett., 68:1858–1861, Mar 1992.

[66] G. A. Bara , E. O. Kane, and M. Schlüter. Theory of the silicon vacancy: An anderson negative-u system. Phys. Rev. B, 21:5662–5686, Jun 1980.

[67] Zhi-Yuan Chen, Yuqian Chen, Q. K. Zhang, X. Q. Tang, D. D. Wang, Z. Q. Chen, P. Mascher, and S. J. Wang. Vacancy-induced ferromagnetic behavior in antiferromagnetic NiO nanoparticles: A positron annihilation study. ECS Journal of Solid State Science and Technology, 6(12):P798–P804, 2017.

[68] N Rinaldi-Montes, P Gorria, D Martínez-Blanco, A B Fuertes, L Fernández Barquín, I Puente-Orench, and J A Blanco. Scrutinizing

the role of size reduction on the exchange bias and dynamic magnetic behavior in NiO nanoparticles. Nanotechnology, 26(30):305705, jul 2015.

[69] N. Rinaldi-Montes, P. Gorria, D. Martínez-Blanco, A. B. Fuertes, L. Fernández Barquín, J. Rodríguez Fernández, I. de Pedro, M. L. Fdez-Gubieda, J. Alonso, L. Olivi, G. Aquilanti, and J. A. Blanco. Interplay between microstructure and magnetism in nio nanoparticles: breakdown of the antiferromagnetic order. Nanoscale, 6:457–465, 2014.

[70] Natalia Rinaldi-Montes, Pedro Gorria, David Martínez-Blanco, Antonio B. Fuertes, Luis Fernández Barquín, Inés Puente-Orench, and Jesús A. Blanco. Bridging exchange bias effect in nio and ni(core)@nio(shell) nanoparticles. Journal of Magnetism and Magnetic Materials, 400:236 – 241, 2016. Proceedings of the 20th International Conference on Magnetism (Barcelona) 5-10 July 2015.